© 2019. Published by The Company of Biologists Ltd | Journal of Cell Science (2020) 133, jcs235416. doi:10.1242/jcs.235416

RESEARCH ARTICLE

SPECIAL ISSUE: CELL BIOLOGY OF THE IMMUNE SYSTEM

FcRn mediates fast recycling of endocytosed albumin and IgG from early macropinosomes in primary macrophages

Wei Hong Toh[1], Jade Louber[1], Ismail S. Mahmoud[1,*], Jenny Chia[2], Greg T. Bass[2], Steve K. Dower[2], Anne M. Verhagen[2] and Paul A. Gleeson[1,‡]

ABSTRACT

The neonatal Fc receptor (FcRn) rescues albumin and IgG from degradation following endocytosis and thereby extends the half-life of these plasma proteins. However, the pathways for the uptake of these soluble FcRn ligands, and the recycling itinerary of the FcRn–ligand complexes, have not been identified in primary cells. Here, we have defined the recycling of human albumin and IgG in primary mouse macrophages selectively expressing the human FcRn. Albumin is internalised by macropinocytosis; in the absence of FcRn, internalised albumin is rapidly degraded, while in the presence of FcRn albumin colocalises to SNX5-positive membrane domains and is partitioned into tubules emanating from early macropinosomes for delivery in transport carriers to the plasma membrane. Soluble monomeric IgG was also internalised by macropinocytosis and rapidly recycled by the same pathway. In contrast, the fate of IgG bound to surface Fcγ receptors differed from monomeric IgG endocytosed by macropinocytosis. Overall, our findings identify a rapid recycling pathway for FcRn ligands from early macropinosomes to the cell surface of primary cells.

KEY WORDS: Neonatal Fc receptor, Albumin, Macropinosome, Recycling

INTRODUCTION

It has long been appreciated that IgG has a long half-life relative to other serum proteins and, in the 1990s, the so-called neonatal IgG Fc receptor (FcRn) was shown to be expressed throughout adult life and to function as a 'protection' receptor that acts by rescuing IgG that had been internalised through endocytosis by endothelial cells from degradation. Subsequently, FcRn was also shown to extend the half-life of serum albumin (Chaudhury et al., 2003). It is now clear that FcRn rescues endocytosed IgG and albumin from lysosomal degradation by capturing these ligands in acidic intracellular compartments, prior to their delivery to lysosomes, and recycling them back to the cell surface, where they dissociate at neutral pH and are released, thereby extending their lifetime within the circulation (Roopenian and Akilesh, 2007; Ward and Ober, 2009). In FcRn-deficient mice, the half-life of IgG and albumin are both reduced to ∼1 day, representing a 4–5-fold reduction for IgG (Roopenian et al., 2003) and a 1.5–2-fold reduction for albumin (Chaudhury et al., 2003). Analysis of clearance rates in conditional FcRn knockout mice demonstrated that endothelial and haematopoietic cells are the major sites of FcRn-mediated IgG homeostasis (Montoyo et al., 2009).

FcRn is a membrane-bound heterodimer consisting of a MHC class I-like heavy chain (∼40 kDa) and a non-covalently associated light chain, β2 microglobulin (β2m) that is common to all MHC class I molecules. FcRn has a classical MHC class I-fold; however, the peptide-binding groove of the α1 and α2 domains is obscured and does not bind peptide ligands (Burmeister et al., 1994a). The IgG-binding site in FcRn involves the α2 and β2m domains of FcRn and pH-dependent salt bridges mediated by two histidine residues of the Fc domain (Burmeister et al., 1994b). The binding site for albumin is on the opposite face of FcRn from the contact sites with Fc and involves a histidine residue (Andersen et al., 2012). FcRn is found in all mammals, although there is species specificity in the interaction with its ligands (Ward and Ober, 2009), a characteristic of the receptor that is relevant to studies of the human ligands in mouse models.

At physiological pH, FcRn does not interact with ligands (Martin et al., 2001). The pH dependence of FcRn binding to ligand defines the intracellular location where the interaction takes place. Albumin is internalised by fluid phase endocytosis, possibly by the efficient macropinocytosis pathway, a pathway highly active in endothelial cells, macrophages and dendritic cells (Lim and Gleeson, 2011; Lim et al., 2015). Cell surface receptors may also be involved in the endocytosis of the FcRn ligands, especially for IgG via Fcγ receptors on haematopoietic cells. Ligands interact with FcRn in the acidic (pH 6.0) endosomal compartments and the complex is recycled to the cell surface where the ligand dissociates from the receptor at neutral pH (Tesar and Björkman, 2010). Analysis of the recycling of IgG and albumin in cell lines, indicates that FcRn recycling occurs via the Rab11 (herein referring to Rab11a and Rab11b forms) recycling endosomes to the plasma membrane (Chia et al., 2018). Live imaging has revealed that GFP-tagged FcRn-positive tubules emanate and break off from endosomal structures, and these tubules are likely to represent transport carriers (Ward et al., 2005). Although these studies using immortalised cells have been informative, the pathways for the uptake of ligand (Anderson, 2014) and recycling, in primary cells is poorly defined. Many studies have investigated internalised IgG by loading the FcRn under acidic conditions, a non-physiological pathway for ligand uptake (Anderson, 2014). Moreover, there have been no reported studies to track the internalisation of albumin by primary cells.

A deeper understanding of the cell biology of ligand uptake pathways in primary cells will assist in a rational approach to the design of recombinant therapeutics that can be recycled via FcRn to extend their half-life (Andersen et al., 2012; Kuo et al., 2010). A key question is whether IgG and albumin share a similar pathway for

[1]The Department of Biochemistry and Molecular Biology and Bio21 Molecular Science and Biotechnology Institute, The University of Melbourne, Victoria 3010, Australia. [2]CSL Limited, Research, Bio21 Molecular Science and Biotechnology Institute, Melbourne, Victoria 3010, Australia.
*Present address: Department of Medical Laboratory Sciences, The Hashemite University, Zarqa, 13133 Jordan.

‡Author for correspondence (pgleeson@unimelb.edu.au)

P.A.G., 0000-0002-5336-6503

Received 18 June 2019; Accepted 16 August 2019

Journal of Cell Science (2020) 133, jcs235416. doi:10.1242/jcs.235416

FcRn–ligand recycling in primary cells or whether there are differences in the uptake and/or recycling pathways. Here, we have analysed the recycling of albumin and IgG in primary mouse macrophages expressing the human FcRn, and have identified a novel fast recycling pathway from early macropinosomes that protects these ligands from degradation.

RESULTS

Albumin is internalised into primary macrophages by macropinocytosis

Macropinocytosis is likely to be the relevant pathway for human serum albumin (HSA) endocytosis *in vivo* as it represents the most efficient form of fluid phase uptake (Lim and Gleeson, 2011; Swanson, 2008). It is important to analyse macropinocytosis in primary cells as this pathway is considerably more efficient in primary cells compared with immortalised cultured cells. Macrophages are considered a major cell type for the recycling of FcRn ligands *in vivo* (Akilesh et al., 2007; Montoyo et al., 2009). Here, we used bone marrow-derived macrophages (BMDM) from a mouse line which harbours a knockout allele of the mouse FcRn α-chain (*Fcgrt*^{tm1Dcr}) and also expresses the human FcRn α-chain cDNA (*FCGRT*), termed mFcRn$^{-/-}$ hFcRn$^{Tg/Tg}$ cells (Roopenian et al., 2010). Previous studies have shown that the hFcRn expressed in the mFcRn$^{-/-}$ hFcRn$^{Tg/Tg}$ mice is functionally active (Petkova et al., 2006; Viuff et al., 2016). This mouse line, mFcRn$^{-/-}$ hFcRn$^{Tg/Tg}$, will be referred to as hFcRn$^{Tg/Tg}$ mice throughout this study. For comparison, an mFcRn$^{-/-}$ mouse line, which lacks FcRn, was also used throughout the study. Antibodies to the α-chain of human FcRn (HPA012122) detected a major band of ∼40 kDa in BMDMs lysates from hFcRn$^{Tg/Tg}$ mice, corresponding to the expected size of the human FcRn heavy chain (Fig. S1). A faint slightly higher Mr band was present in the mFcRn$^{-/-}$ sample stained with HPA012122 antibodies; however, this faint band was non-specific as it was not detected with another antibody to the human FcRn heavy chain (B-8 antibodies) (data not shown). Immunofluorescence staining of macrophages from hFcRn$^{Tg/Tg}$ mice showed that hFcRn was predominantly localised to punctate and donut-like structures through the cytoplasm (Fig. S1), whereas no staining was observed in mFcRn$^{-/-}$ or wild-type BMDMs (Fig. S1). Collectively, these findings indicate that HPA012122 antibodies are specific for hFcRn.

We analysed Alexa Fluor 488-conjugated HSA (HSA–AF488) uptake in BMDMs and observed intense intracellular fluorescence with 100 µg/ml HSA–AF488 after 15 min uptake at 37°C (Fig. S1C). BMDMs were then incubated with both HSA–AF488 and a known marker for uptake into macropinosomes, namely 70 kDa dextran conjugated to TxRed, as 70 kDa dextran is predominantly internalised by macropinocytosis (Kerr et al., 2006; Lim et al., 2012, 2008). After incubation at 37°C for 15 min, HSA–AF488 was detected in the large structures (0.2–2 µm in diameter), a size compatible with the size of macropinosomes, which were also positive for TxRed-conjugated dextran (Fig. 1A), in both hFcRn$^{Tg/Tg}$ (Fig. 1A) and mFcRn$^{-/-}$ cell (data not shown). The level of uptake of the HSA–AF488 by hFcRn$^{Tg/Tg}$ or mFcRn$^{-/-}$ BMDMs was very similar, as quantified by flow cytometry (Fig. 1D), indicating that the FcRn is not required for initial uptake of the albumin. Moreover, the uptake of HSA–AF488 by hFcRn$^{Tg/Tg}$ or mFcRn$^{-/-}$ BMDMs was dramatically reduced (>70% reduction) after treatment with the selective macropinosome inhibitor 5-(N-ethyl-N-isopropyl) amiloride (Koivusalo et al., 2010; West et al., 1989), as assessed by flow cytometry and immunofluorescence, confirming the identity of the large endosomes as macropinosomes (Fig. 1B,C).

Internalised albumin is rapidly degraded in BMDMs lacking FcRn

Next, we determined the fate of endocytosed HSA in BMDM with and without hFcRn by performing a 15 min pulse with 100 µg/ml HSA–AF488 followed by a chase. Surprisingly, we found that by the end of the 15 min chase, the intracellular HSA–AF488 fluorescence had dramatically waned with very little detected in either hFcRn$^{Tg/Tg}$ or mFcRn$^{-/-}$ BMDMs (Fig. 2A, HSA only). To determine whether degradation was contributing to the loss of fluorescence, particularly in the mFcRn$^{-/-}$ cells, we treated cells with a cocktail of protease inhibitors throughout the pulse and the chase. The fluorescence in the protease inhibitor-treated cells was maintained in the mFcRn$^{-/-}$ cells, as assessed by confocal microscopy and flow cytometry (Fig. 2A,C,E), indicating that the internalised HSA–AF488 was rapidly degraded in the mFcRn$^{-/-}$ BMDMs (Fig. 2A,E). To directly analyse the proteolytic degradation of internalised HSA, we used DQ-Red-tagged BSA (DQ–BSA), a self-quenched conjugate of albumin that exhibits fluorescence at 620 nm upon proteolytic degradation in the late endosome/lysosome (Daro et al., 2000; Santambrogio et al., 1999). BMDMs from mFcRn$^{-/-}$ mice were pulsed with both HSA–AF488 and DQ–BSA for 15 min and then chased at 37°C for 10 min. After the 15 min pulse, HSA–AF488 was detected in large macropinosomes, whereas there was minimum fluorescence at 620 nm (Fig. 3A). After the 10 min chase, there was a very strong signal at 620 nm in endosomal structures dispersed throughout the cytoplasm of CSF-1-treated BMDMs (Fig. 3A). These DQ-Red-positive structures showed extensively colocalisation with HSA–AF488. HSA–AF488 was also detected in very large endosomal structures devoid of 620 nm fluorescence, and these large structures were located in the periphery of the cell (Fig. 3B, arrows). These findings demonstrate, first, that albumin is rapidly degraded in activated BMDMs in the absence of FcRn, and second, that the proteolytic degradation of DQ–BSA occurs downstream of the large early macropinosomes, most likely after subsequent fusion of the maturing macropinosomes with late endosomes (Kerr et al., 2006). Thus, for FcRn to rescue HSA from degradation, the receptor must bind and divert the ligand in the early stages of the macropinosome pathway.

FcRn mediates rapid recycling of internalised albumin-activated macrophages

In contrast to mFcRn$^{-/-}$ BMDM, following endocytosis of HSA–AF488 in hFcRn$^{Tg/Tg}$ BMDM, the fluorescent signal rapidly disappeared (by 15 min), regardless of the presence or absence of protease inhibitors, as assessed by optical microscopy and flow cytometry (Fig. 2A,C,E). In addition, DQ–BSA internalised by hFcRn$^{Tg/Tg}$ BMDM showed a minimal signal at 620 nm after a 10 min chase (Fig. 3A); as BSA can interact strongly with the human FcRn (Chaudhury et al., 2003), this finding indicates that BSA is protected from degradation in the presence of FcRn. To determine whether the disappearance of fluorescence was due to FcRn recycling, we incubated hFcRn$^{Tg/Tg}$ BMDMs with a previously defined FcRn non-binding HSA mutant, rHSA^{H464Q}-AF488 (Andersen et al., 2012). In contrast to the disappearance of wild-type HSA, this non-binding HSA mutant showed strong intracellular fluorescence after 15 min chase in the presence of protease inhibitors, and regardless of the presence or absence of FcRn (Fig. 2B,D,F), indicating the recycling of wild-type HSA was promoted by FcRn. To assess recycling and secretion of HSA, we analysed cell lysates and the extracellular medium for HSA by immunoblotting. Similar levels of HSA were detected in cell lysates after the pulse, regardless of the presence or absence of FcRn or whether wild-type or mutant

Journal of Cell Science (2020) 133, jcs235416. doi:10.1242/jcs.235416

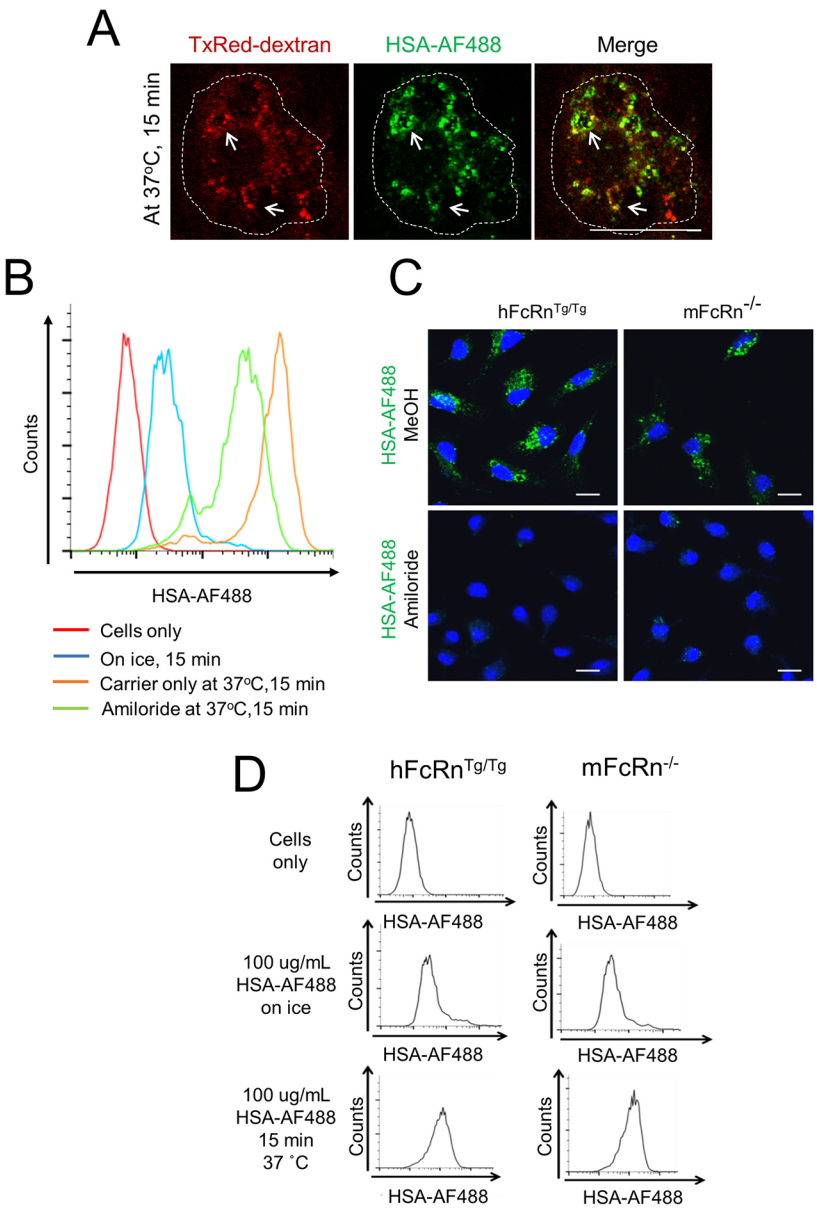

Fig. 1. Co-uptake of HSA–AF488 and TxRed–dextran in BMDMs and inhibition by amiloride. (A) BMDMs were incubated with 200 µg/ml HSA–AF488 and 500 µg/ml lysine-fixable TxRed-conjugated 70 kDa dextran (TxRed–dextran) at 37°C for 15 min. Macropinosomes are indicated by white arrows, and the edge of the cell with a dashed line. (B,C) Effect of amiloride on HSA–AF488 internalisation in BMDMs. BMDMs derived from mFcRn$^{-/-}$ or hFcRn$^{Tg/Tg}$ mice were either pre-treated with 100 µM of 5-(N-ethyl-N-isopropyl) amiloride or 1.5% methanol (carrier control treatment) at 37°C for 30 min, followed by incubation with HSA–AF488 (200 µg/ml) at 37°C for 15 min. Cells were then either fixed and analysed by immunofluorescence microscopy (C), or were washed and analysed directly, without fixing, by FACS (B), to quantify the amount of HSA–AF488 internalisation in BMDMs derived from hFcRn$^{Tg/Tg}$ mice. (D) FACS analysis to quantify the internalisation of HSA–AF488 in BMDMs derived from hFcRn$^{Tg/Tg}$ or mFcRn$^{-/-}$ mice. BMDMs were incubated with HSA–AF488 for 15 min. Note the similar level of HSA–AF488 uptake by both hFcRn$^{Tg/Tg}$ and mFcRn$^{-/-}$ BMDMs. Scale bars: 5 µm.

HSA was endocytosed (Fig. 4). Elevated levels of HSA, representing 50% of total endocytosed HSA, were detected in the media from hFcRn$^{Tg/Tg}$ BMDM after the 15 min chase period compared with media from mFcRn$^{-/-}$ cells (Fig. 4A,B). In addition, only low levels (1–2%) of the non-binding HSA mutant, rHSA^{H464Q}–AF488, were detected in the medium of hFcRn$^{Tg/Tg}$ BMDMs after the chase period (Fig. 4C,D). Thus, hFcRn$^{Tg/Tg}$ BMDMs were able to recycle wild-type HSA, but not the non-binding mutant, rapidly into the medium after endocytosis, whereas mFcRn$^{-/-}$ BMDMs were not.

Albumin is recycled to the cell surface directly from early macropinosomes

We next investigated the mechanism for HSA recycling from macropinosomes. Macropinosomes are known to tubulate extensively during maturation, and the tubules pinch off to become transport carriers (Kerr et al., 2006). The destinations of these macropinosome-derived transport carriers are not well defined, but have been proposed to be involved in recycling. To assess whether HSA entered tubules derived from macropinosomes, HSA–AF488 pulsed BMDMs were fixed under conditions that preserve the tubular structures, namely with 2% PFA. HSA–AF488 was detected in abundant tubules arising from large Alexa Fluor 488-positive macropinosomes in hFcRn$^{Tg/Tg}$ BMDMs (Fig. 5A). In contrast, very few HSA–AF488-labelled tubules were visible in mFcRn$^{-/-}$ BMDMs (Fig. 5A) or with the non-binding HSA^{H464Q} mutant in hFcRn$^{Tg/Tg}$ BMDM (data not shown). In both cases the labelled HSA–AF488 was restricted to the body of large macropinosomes, indicating that the partitioning of the soluble HSA into tubules is mediated by the membrane FcRn.

The intracellular location of FcRn was also analysed in activated hFcRn$^{Tg/Tg}$ BMDM. Intracellular staining required fixation conditions which results in the loss of the tubular domains; however, SNX5 provides a marker for newly formed macropinosomes and is also associated with a subdomain that generates the tubular extensions (Kerr et al., 2006). Dual staining for SNX5 and FcRn in hFcRn$^{Tg/Tg}$ BMDM revealed extensive colocalisation of FcRn with SNX5 in large macropinosome-like structures. Quantitative analysis

Journal of Cell Science (2020) 133, jcs235416. doi:10.1242/jcs.235416

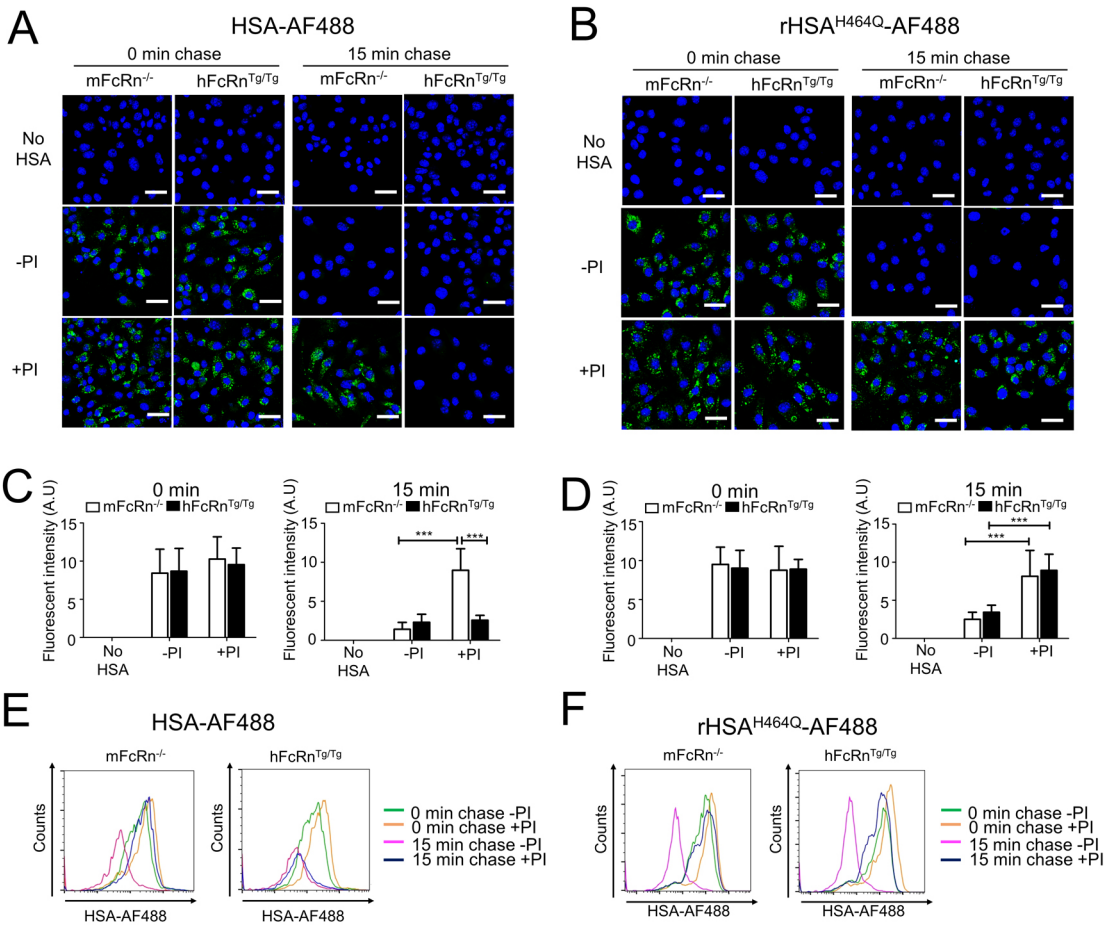

Fig. 2. HSA is rapidly degraded in mFcRn$^{-/-}$ BMDMs. (A–F) mFcRn$^{-/-}$ and hFcRn$^{Tg/Tg}$ BMDMs were plated in eight-well chamber slides and in C-RPMI supplemented with mCSF-1 for 3 days. BMDMs were then rendered quiescent by culturing overnight in C-RPMI in the absence of mCSF-1. The next day BMDMs were incubated in C-RPMI supplemented with either protease inhibitors or 0.01% DMSO (carrier control) for 4.5 h. Cells were then washed with PBS and incubated with 100 µg/ml HSA–AF488 or HSA^{H464Q}–AF488 in the presence or absence of protease inhibitors in serum-free medium (SFM) supplemented with 50 ng/ml mCSF-1 for 15 min. Cell monolayers were washed in PBS and HSA was chased in SFM containing either protease inhibitors (PI) or DMSO (carrier control) for 15 min. Cells were fixed in 4% PFA at 0 min and 15 min chase time points. (A,B) Confocal microscopy images of mFcRn$^{-/-}$ and hFcRn$^{Tg/Tg}$ BMDMs at 0 min and 15 min showing (A) HSA–AF488 (green), or (B) HSA^{H464Q}–AF488 (green) and DAPI (blue). (C,D) Fluorescent intensity of mFcRn$^{-/-}$ and hFcRn$^{Tg/Tg}$ BMDMs containing (C) HSA–AF488 or (D) HSA^{H464Q}–AF488 at 0 and 15 min chase time points. Data at each time point is from 50 cells over three independent experiments. Error bars show mean±s.e.m. ***P<0.001 (unpaired two-tailed t-test). (E,F) mFcRn$^{-/-}$ and hFcRn$^{Tg/Tg}$ BMDMs containing (E) HSA–AF488 or (F) HSA^{H464Q}–AF488 at 0 and 15 min chase time points. Total fluorescence of cells was analysed by FACS. A.U, arbitrary units. Scale bars: 10 µm.

indicated that >50% of FcRn colocalised with SNX5. EEA1, a marker for early endosomes, is also recruited to early macropinosomes. Approximately 30% of FcRn also colocalised with EEA1, whereas <12% colocalised with Rab11, a marker of recycling endosomes (Fig. 5B). These results demonstrate that FcRn is predominantly present in large macropinosome structures, and therefore FcRn has the potential to mediate binding and recycling from newly formed macro structures.

Next, we analysed the relationship between the localisation of the ligand HSA and the receptor FcRn over a 10 min chase period (Fig. 5D). After a 15 min pulse with HSA–AF488 there was a 50% colocalisation of HSA with FcRn indicating that the ligand and receptor were in close proximity very early after fluid phase uptake. The association remained high throughout the 10 min chase. BMDMs from mFcRn$^{-/-}$ had no staining with the antibody to FcRn, as expected (Fig. 5C). We then analysed the level of colocalisation of HSA ligand with SNX5, Rab11 and Lamp1 over a 10 min chase to identify the intracellular trafficking pathway for HSA–AF488 (Fig. 5D–F). In hFcRn$^{Tg/Tg}$ BMDMs, there was a high level of colocalisation of ligand with SNX5, whereas in the absence of hFcRn, the colocalisation with SNX5 was only ∼10% (Fig. 5D). Thus, the presence of the hFcRn resulted in localisation of HSA to SNX5 domains, a relevant finding as SNX5 domains are considered to generate the tubules for cargo recycling. Only small amounts of ligand was associated with either Rab11 or Lamp1 over the 10 min pulse in the presence of hFcRn (Fig. 5E,F), indicating that the majority of ligand did not enter either recycling endosomes or late endosomes/lysosomes. In contrast, in the absence of hFcRn, HSA–AF488 showed only low levels (∼10%) of colocation with SNX5, and high levels of colocalisation with Lamp1. The colocalisation of HSA with the late endosome/lysosome marker in the absence of FcRn increases over the 10 min chase period, indicating delivery of HSA ligand to the lysosomes. Therefore, taken together, in mFcRn$^{-/-}$ BMDM, HSA–AF488 was restricted to the body of the large endosomes and transported rapidly to lysosomes. In hFcRn$^{Tg/Tg}$ BMDMs, however, HSA was detected on abundant tubules emerging from large endosomes, and colocalised with FcRn and SNX5 subdomains, whereas very little was directed towards lysosomes.

Journal of Cell Science (2020) 133, jcs235416. doi:10.1242/jcs.235416

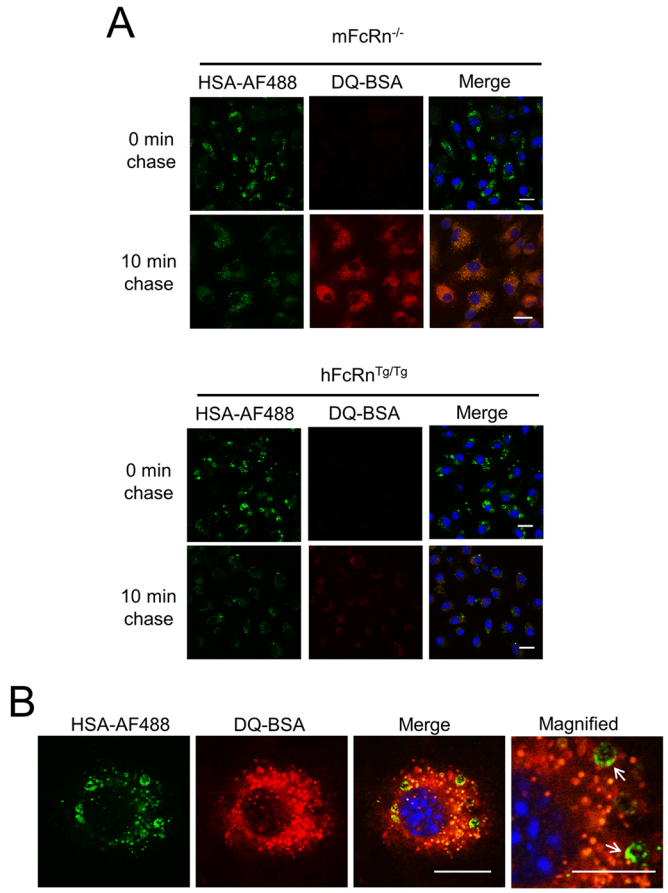

Fig. 3. Internalised albumin is rapidly degraded in lysosomes in mFcRn$^{-/-}$ BMDMs. (A,B) mFcRn$^{-/-}$ and hFcRn$^{Tg/Tg}$ BMDMs were plated in eight-well chamber slides and rendered quiescent by culturing overnight in C-RPMI in the absence of mCSF-1. Cells were then incubated with 100 µg/ml HSA–AF488 and DQ–BSA in serum-free medium (SFM) supplemented with 50 ng/ml mCSF-1 for 10 min. BMDMs were subsequently washed in PBS and HSA–AF488 and DQ–BSA were chased in SFM for 10 min. Cells were fixed in 4% PFA at the 0 min and 10 min chase time points. (A) Confocal microscopic images of mFcRn$^{-/-}$ and hFcRn$^{Tg/Tg}$ BMDMs at 0 min and 10 min showing HSA–AF488 (green), DQ–BSA (red) and DAPI (blue). (B) High-magnification image of an mFcRn$^{-/-}$ BMDM cell at the 10 min time point showing HSA–AF488 (green), DQ–BSA (red) and DAPI (blue). Arrows indicate HSA–AF488-positive macropinosomes devoid of 620 nm fluorescence. Scale bars: 10 µm.

To directly visualise tubules emerging from early macropinosomes we performed live imaging of BMDMs following a 5 min pulse with HSA–AF488 (Fig. 6). In hFcRn$^{Tg/Tg}$ BMDM imaging revealed dynamic formation of fluorescently labelled tubules emerging from large structures in the periphery of the cell. These tubular structures were highly mobile and projected towards the cell surface where the fluorescence intensity then waned, indicating delivery of the fluorescent cargo to the plasma membrane (PM) (Movie 1). In contrast, very few HSA–AF488 tubules were observed in mFcRn$^{-/-}$ BMDM (Fig. 6A; Movie 2). We analysed >10,000 Alexa Fluor 488 tracks in hFcRn$^{Tg/Tg}$ BMDMs and mFcRn$^{-/-}$ BMDMs, collected randomly from the total intracellular HSA–AF488 pool and included both endosomal and tubular structures. The Alexa Fluor 488 tracks showed a higher mean displacement and speed in hFcRn$^{Tg/Tg}$ BMDMs compared with that in mFcRn$^{-/-}$ BMDMs (Fig. 6C–E). This quantitative analysis data confirms that the HSA–AF488 was associated with more-dynamic structures, which moved across longer distances in hFcRn$^{Tg/Tg}$ BMDM compared with mFcRn$^{-/-}$ BMDMs. We then compared the behaviour of the non-binding rHSA^{H464Q}–AF488 mutant in live BMDMs. Very few rHSA^{H464Q}–AF488-labelled tubules were visualised in either hFcRn$^{Tg/Tg}$ BMDM or mFcRn$^{-/-}$ BMDMs (Fig. 6B, Movies 3 and 4). Moreover, analysis of Alexa Fluor 488 tracks in hFcRn$^{Tg/Tg}$ BMDMs and mFcRn$^{-/-}$ BMDMs showed no difference in the displacement and speed of rHSA^{H464Q}–AF488 (Fig. 6C–E). This data suggests that HSA–AF488 is only recruited into tubules once bound to FcRn. To exclude the unlikely possibility that tubules are dependent on FcRn-bound ligand for their formation, we labelled the membranes of early macropinosomes in mFcRn$^{-/-}$ BMDMs by use of the PM label CellMask Deep Red, to visualise the membranes of emerging tubules. After PM labelling with CellMask Deep Red and uptake of HSA–AF488, the HSA ligand was observed in CellMask Deep Red-labelled large macropinosomes close to the PM (Fig. S2). Live imaging revealed CellMask Deep Red-labelled tubules emanating from the HSA–AF488-positive macropinosomes (Movie 5, Fig. S2). The CellMask Deep Red-labelled tubules were devoid of HSA-AF488 in the FcRn$^{-/-}$ BMDM (Fig. S2), demonstrating that the tubules form independently of FcRn and its ligand. Hence, collectively these data demonstrate that HSA–AF488 is recruited into dynamic tubules emerging from early macropinosomes in FcRn-dependent manner.

Monomeric IgG is excluded from endocytosis by binding to Fcγ

A question that arises from these findings, is whether IgG follows a similar intracellular pathway to that of albumin in activated macrophages, given that IgG is not only a ligand of FcRn but also for Fcγ receptors, which have a role in delivery of immunoglobulin–antigen complexes to the MHCII loading compartments for antigen presentation. To compare the transport routes of albumin and IgG, BMDMs were pulsed with 100 µg/ml HSA–AF488 and Alexa Fluor 594-conjugated IgG (IgG–AF594) simultaneously for 15 min in the presence and absence of protease inhibitors. As expected, with a 0 min chase, HSA–AF488 was detected in large macropinosomes in BDMDs treated with either carrier only or with protease inhibitors. The majority of the IgG was associated with the cell surface, with only low levels colocalised with internalised HSA–AF488. After the 15 min chase, the HSA–AF488 signal was greatly reduced in both FcRn$^{-/-}$ BMDMs and hFcRn$^{Tg/Tg}$ BMDMs whereas the IgG–AF594 persisted, as assessed by confocal microscopy (Fig. 7A) and also by flow cytometry of BMDM pulsed with 100 µg/ml IgG–AF488 alone (Fig. 7B). To assess whether Fcγ was responsible for cell surface binding and persistence, we treated BMDMs with mouse serum to block the surface Fcγ receptors (Fig. S3) and repeated the uptake experiment with both ligands. Mouse IgG binds (and blocks) Fcγ receptors but is unable to interact with human FcRn. At the end of the 15 min pulse (0 min chase), both Alexa Fluor ligands were detected in large macropinosomes and showed extensive overlap (Fig. 7A). After the 15 min chase, very little signal was detected in the absence of protease inhibitors regardless of the presence or absence of FcRn. In the presence of protease inhibitors there remained a strong signal for both ligands in FcRn$^{-/-}$ BMDM whereas the signals were very weak in hFcRn$^{Tg/Tg}$ BMDMs (Fig. 7A). Analysis by flow cytometry of BMDMs pulsed with solely IgG–AF488 confirmed these observations; there was a dramatic reduction in signal in hFcRn$^{Tg/Tg}$ BMDMs even in the presence of protease inhibitors (Fig. 7B). Hence, if the Fcγ is blocked or saturated by unlabelled mouse IgG, the internalisation of monomeric IgG by fluid phase macropinocytosis is more readily observed and the IgG

Journal of Cell Science (2020) 133, jcs235416. doi:10.1242/jcs.235416

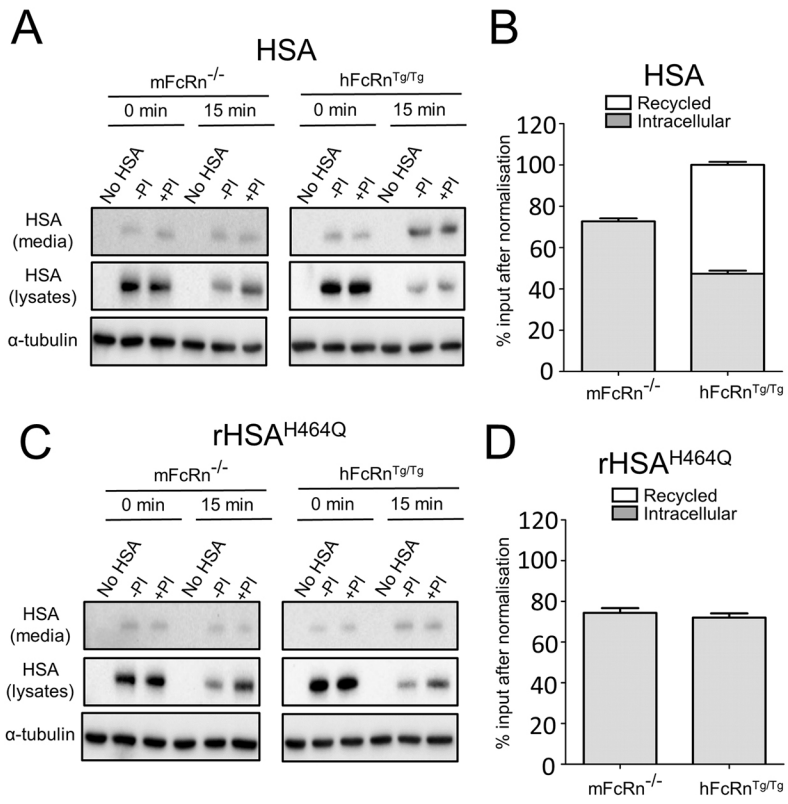

Fig. 4. HSA is rapidly recycled out of the cell in hFcRn$^{Tg/Tg}$ BMDMs and rapidly degraded in mFcRn$^{-/-}$ BMDMs. (A,C) Immunoblotting of conditioned medium and cell extracts of mFcRn$^{-/-}$ and hFcRn$^{Tg/Tg}$ BMDMs pulsed with either (A) HSA–AF488 or (C) HSA^{H464Q}–AF488 for 0 or 15 min and probed with goat anti-HSA and mouse anti-α-tubulin antibodies, using a chemiluminescence detection system. (B,D) Bar graph of the densitometric quantification of HSA bands (15 min uptake in the presence of protease inhibitors) after normalisation to the density of the α-tubulin bands and cell lysate input. The density of the HSA from the conditioned medium at the end of the pulse period and following washing (0 min chase) represents background, and was subtracted from the HSA bands of the chase samples. Densitometry of the bands was performed using ImageJ. Data was expressed as the percentage recycled (using band intensities from conditioned medium) versus percentage intracellular (using band intensities from cell lysate) for both mFcRn$^{-/-}$ and hFcRn$^{Tg/Tg}$ BMDMs, and HSA–AF488 (B) or HSA^{H464Q}–AF488 (D). Data was pooled from three independent experiments and is expressed as the mean±s.e.m.

internalised by this pathway follows similar FcRn-dependent trafficking kinetics to albumin.

DISCUSSION

The physiological pathways for uptake and recycling of FcRn ligands in primary cells are poorly defined (Anderson, 2014). Here, we have shown that the fluid phase uptake of albumin and IgG by primary macrophages is predominantly undertaken by macropinocytosis and have identified a rapid recycling pathway for albumin from newly formed macropinosomes. Our study demonstrates that FcRn mediates the rapid recycling directly from newly formed macropinosomes in activated macrophages because: (1) ∼50% HSA is recycled into the cell culture within 15 min of internalisation; (2) HSA is detected in tubules emerging from early macropinosomes which were then directed towards the PM; (3) in the absence of FcRn, HSA is neither partitioned into tubules nor recycled, but remains within the body of the macropinosome and is subsequently rapidly degraded; (4) the non-FcRn-binding mutant of HSA, rHSA^{H464Q}–AF488, is rapidly internalised and degraded in hFcRn$^{Tg/Tg}$ BMDM, and is not recycled into the culture medium and (5) in fixed BMDMs, FcRn is detected in SNX5 subdomains of the newly formed macropinosomes, domains known to give rise to tubular carriers (Kerr et al., 2006). We also demonstrated that monomeric IgG taken up by fluid phase endocytosis follows a similar pathway to that of albumin.

Macropinocytosis is the major pathway for uptake of HSA by primary macrophages, as demonstrated by the colocalisation with the fluid phase marker of macropinocytosis 70 kDa dextran, into very large endocytic structures and the reduction of HSA endocytosis with amiloride, a selective inhibitor of this pathway (Koivusalo et al., 2010). Macropinosomes are generated from actin-mediated ruffling of the PM. Recent studies have identified two distinct pathways of macropinocytosis in macrophages, wherein macropinosomes are derived from peripheral ruffles or derived from dorsal ruffles following receptor activation (Condon et al., 2018; Lim et al., 2015). Dorsal ruffles give rise to larger macropinosomes than peripheral ruffles (Condon et al., 2018; Lim et al., 2015). Our previous studies have shown that the majority of macropinosomes from activated macrophages are derived from these dorsal ruffles (Lim et al., 2015). Newly formed macropinosomes are known to tubulate extensively, a process dependent on SNX5 and other Bar domain proteins (Kerr et al., 2006). These membrane tubules are precursors of transport carriers considered to transport cargoes to other intracellular destinations. Recycling of membrane cargo, endocytosed by macropinocytosis, back to the PM has been previously demonstrated (Bryant et al., 2007), although the relationship between the early tubulation events and cell surface recycling has not been previously demonstrated. The findings in this paper show that newly formed macropinosomes undergo extensive tubulation, a process involving removal of membrane from the early macropinosome, followed by acquisition of proteolytic enzyme activity, presumably by the maturing macropinosome body fusing with late endosomes/lysosome compartments.

In the absence of FcRn, or the inability to bind FcRn, HSA was rapidly degraded. Activated macrophages have been reported previously to be able to very rapidly (within 10 min) degrade endocytosed soluble proteins (Diment and Stahl, 1985). The FcRn-dependent partitioning of HSA into tubules of the newly formed macropinosomes provides a mechanism to rapidly remove the ligand from the maturing macropinosome body and protect it from proteolytic degradation. The use of self-quenched DQ–BSA showed that newly formed macropinosomes did not proteolytically digest albumin; however, within 10 min of chase following internalisation of DQ–BSA by FcRn$^{-/-}$ BMDMs, the self-quenched DQ–BSA showed fluorescence at 620 nm, indicating that the soluble conjugate was exposed to a degradative environment. Our findings are consistent with previous studies, which showed that BSA is rapidly degraded by

Journal of Cell Science (2020) 133, jcs235416. doi:10.1242/jcs.235416

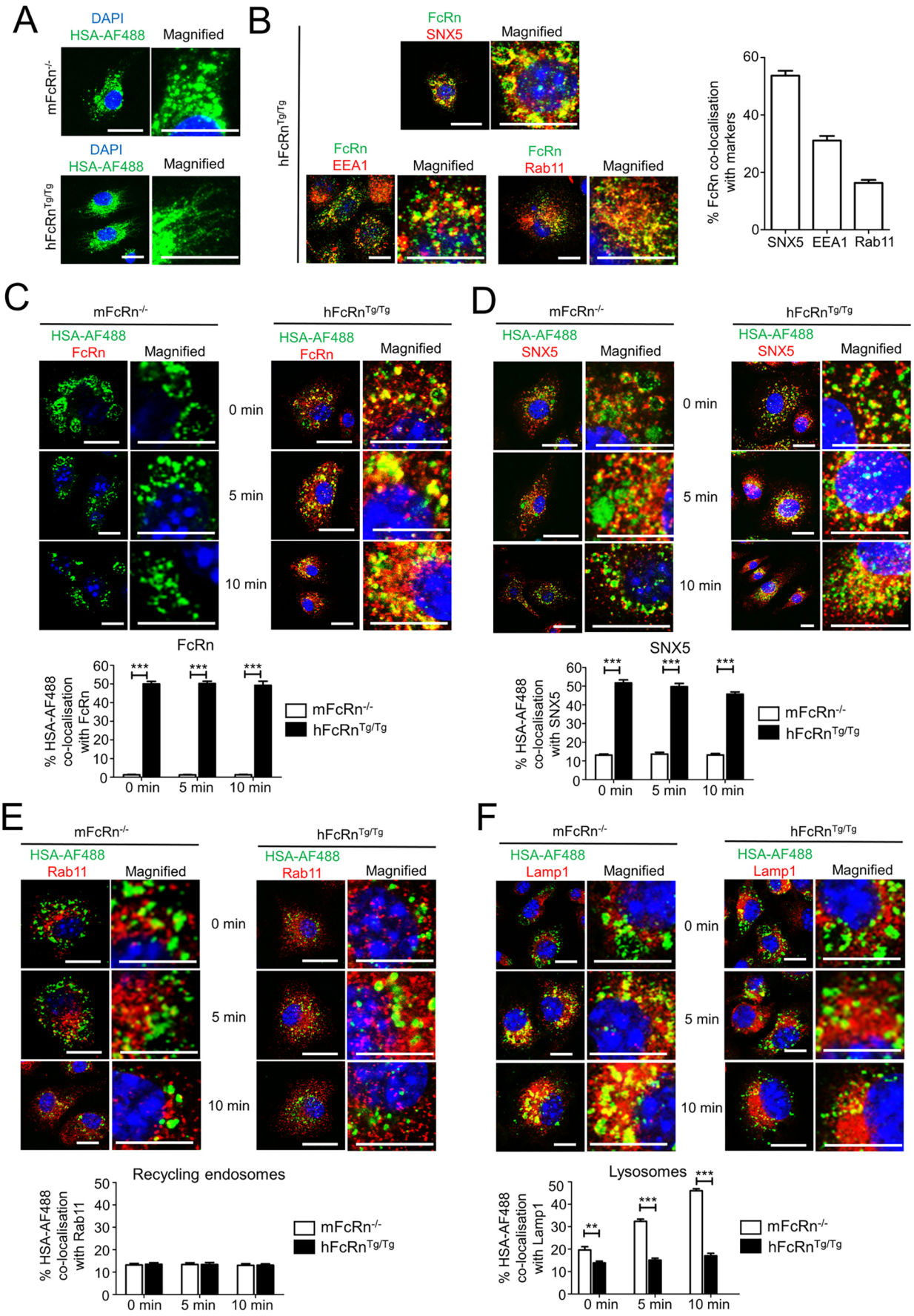

Fig. 5. See next page for legend.

Journal of Cell Science (2020) 133, jcs235416. doi:10.1242/jcs.235416

Fig. 5. Analysis of intracellular trafficking pathways of internalised HSA. (A–F) mFcRn$^{-/-}$ and hFcRn$^{Tg/Tg}$ BMDMs were plated in eight-well chamber slides and rendered quiescent by culturing overnight in C-RPMI in the absence of mCSF-1. Cells were then incubated in C-RPMI supplemented with either protease inhibitors (PI) or 0.01% DMSO (carrier control) for 4.5 h, washed with PBS, and incubated with 100 µg/ml HSA–AF488 in the presence or absence of protease inhibitors in serum-free medium supplemented with 50 ng/ml mCSF-1 for 10 min. BMDMs were subsequently washed in PBS and HSA was chased in serum-free medium (SFM) for 15 min. Cells were fixed in (A) 2% PFA or (B–F) 4% PFA at the 0 min, 5 min and 10 min chase time points. (A) Confocal images of HSA–AF488 (green) and DAPI (blue) in mFcRn$^{-/-}$ and hFcRn$^{Tg/Tg}$ BMDMs after 10 min chase. (B) Confocal images of FcRn (green) and organelle markers (red), SNX5, EEA1 and Rab11. The percentage of FcRn in macropinosomes, early endosomes and recycling endosomes at the 10 min time point was calculated from the percentage of total FcRn pixels that overlapped with SNX5, EEA1 or Rab11, respectively. All calculations were performed using the OBCOL plugin on ImageJ. Data represents the mean ±s.e.m. from three independent experiments, where for each experiment, an average value was determined from two to five images (each containing eight or more cells) for each time point. (C–F) Confocal images of HSA–AF488 (green) and markers (red) as follows: (C) FcRn, (D) SNX5, (E) Rab11 or (F) Lamp1. The percentage of HSA–AF488 colocalised with SNX5 (macropinosomes) and FcRn, and in recycling endosomes (Rab11) and lysosomes (Lamp1) following 0, 5 or 10 min chase periods was calculated from the percentage of total HSA-AF488 pixels that overlapped with FcRn, SNX5, Rab11 or Lamp1, respectively. All calculations were performed using the OBCOL plugin on ImageJ. Data represent the mean±s.e.m. from three independent experiments, where for each experiment, an average value was determined from two to five images (each containing eight or more cells) for each time point. **P<0.01, ***P<0.001 (unpaired two-tailed t-test). Scale bars: 10 µm.

macrophages after internalisation (Diment and Stahl, 1985). Hence, to be protected from degradation, cargo must be removed rapidly from the newly formed macropinosome. The tubules emanating from newly formed macropinosomes allow the receptor and cargos to be returned to the PM instead of being subject to proteolytic digestion. Indeed, this is the first example in which we are aware of a receptor which is directly recycled from newly formed macropinosomes back to the PM. A model summarising our findings is shown in Fig. 8.

What is the source of the FcRn in early macropinosomes? Given the very rapid recycling of albumin, it is likely that hFcRn is internalised from the cell surface via membrane ruffles, as proposed in the model depicted in Fig. 8. An acidic environment is required for binding of FcRn to ligand. Following their biogenesis in macrophages, macropinosomes are known to shrink and acidify (Racoosin and Swanson, 1989; Swanson and Watts, 1995). It was recently reported that the WASH complex regulates V-ATPase trafficking on macropinosomes as an early event in macropinosome maturation in *Dictyostelium* (Buckley et al., 2016). Hence, it is possible a similar process occurs in mammalian macrophages to acidify early macropinosomes. Also of note is that very little Rab11 colocalised with albumin during recycling in these activated macrophages, indicating that the recycling pathway is independent of Rab11. This finding is in contrast to what is seen in cells that do not have a high macropinocytic activity, where recycling of FcRn-bound ligand occurs via Rab11 recycling endosomes (Chia et al., 2018). Sorting signals have been identified in the cytoplasmic tail of FcRn that are required for transport of FcRn from early endosomes to recycling endosomes (Mahmoud et al., 2017). An interesting question concerns the mechanism for sorting of FcRn into the tubular membranes of the early macropinosomes. One possibility is that this could involve similar sorting machinery to that used in the early endosome tubulation process (Cullen and Steinberg, 2018). However, of note is that Rab4, which is considered to regulate rapid recycling back from early endosomes back to the PM (Maxfield and McGraw, 2004; van der Sluijs et al., 1992), does not colocalise with internalised HSA in early macropinosomes (W.H.T. and P.A.G., unpublished data), indicating that the transport route is Rab4 independent. Other possible candidates for the recycling machinery could include SNX17 (McNally et al., 2017; van Kerkhof et al., 2005), SNX27 (Steinberg et al., 2013), and the retromer (Cullen and Steinberg, 2018) and retriever complexes (McNally et al., 2017). The challenge will be to now define the trafficking machinery involved in this transport pathway in primary macrophages.

Our results also provide a basis for understanding the intracellular itinerary and fate of IgG endocytosed by antigen-presenting cells, depending on whether IgG is monomeric or exists in an immune complex. IgG is not only a ligand of FcRn but also for Fcγ receptors, which have a role in delivery of immunoglobulin–antigen complexes to the MHCII-loading compartments for antigen presentation (Guilliams et al., 2014; Molfetta et al., 2014). Given the concentration of IgG in the circulation, the bulk of the monomeric IgG that enters macrophages will be via macropinocytosis and, based on our findings in this paper, will be recycled by the same FcRn mechanism as albumin. Our data also demonstrated that monomeric IgG bound to surface Fcγ receptors has a long residency time at the PM. On the other hand, immune complexes bind to Fcγ receptors, induce rapid uptake via clathrin-mediated endocytosis (Molfetta et al., 2014) and are delivered to lysosomes, hence avoiding the rapid transport pathway mediated by FcRn in early macropinosomes (Fig. 8B). Internalised complexes may be exposed to FcRn in early or late endosomes and an interaction in these compartments cannot be excluded. Nonetheless, the model proposed in Fig. 8B allows for immune complexes to be delivered to late endosomes and the antigen processing compartment independently of the rapid FcRn recycling pathway identified in this paper. Thus, even though monomeric IgG and IgG–antigen complexes are both potential ligands for FcRn, they are internalised by distinct mechanisms, which in turn determines their intracellular transport fate.

Overall our studies demonstrate the importance of defining FcRn recycling pathways in primary cells. The characteristics of recycling of both albumin and IgG could be relevant for the design of recombinant protein therapeutics that seek to exploit the FcRn pathway for potential half-life extension, notwithstanding that the properties of any particular recombinant protein therapeutic will need to be determined.

MATERIALS AND METHODS

Antibodies and reagents

Rabbit polyclonal antibodies to FcRn (#HPA012122; 1:200) and protease inhibitors (P1860) were purchased from Sigma-Aldrich. Mouse monoclonal anti-human FcRn (B-8, sc-271745; 1:200) was purchased from Santa Cruz Biotechnology Inc. Goat anti-HSA (#EHALB; 1:600) was purchased from Thermo Fisher Scientific. Lysine-fixable TxRed-conjugated 70 kDa dextran was purchased from Invitrogen (Thermo Fisher Scientific). Rat anti-mouse Lamp1 (#553792, Clone 1D4B; 1:600) was purchased from BD Transduction Laboratories. Rabbit polyclonal anti-Rab11 (#5589; 1:200) and anti-EEA1 (#2411; 1:200) were purchased from Cell Signaling Technology. Mouse antibodies to α-tubulin (Clone 236-10501; 1:5000), DQ-Red BSA (#D12051) and DAPI were purchased from Life Technologies. mCSF-1 (GF053) was purchased from Merck Millipore. Lab-generated rabbit anti-mouse SNX5 antibody has been described previously and was used at 1:1000 (Lim et al., 2012). Secondary antibodies used for immunofluorescence were goat anti-rabbit-IgG conjugated to Alexa Fluor 568 nm, goat anti-rabbit-IgG conjugated to Alexa Fluor 488 nm, goat anti-mouse-IgG conjugated to Alexa Fluor 568 nm and goat anti-mouse-IgG conjugated to Alexa Fluor 488 nm were purchased from Life Technologies. Horseradish peroxidase (HRP)-conjugated sheep anti-rabbit-Ig, anti-mouse-Ig and donkey anti-goat-Ig were purchased from DAKO Corporation

Journal of Cell Science (2020) 133, jcs235416. doi:10.1242/jcs.235416

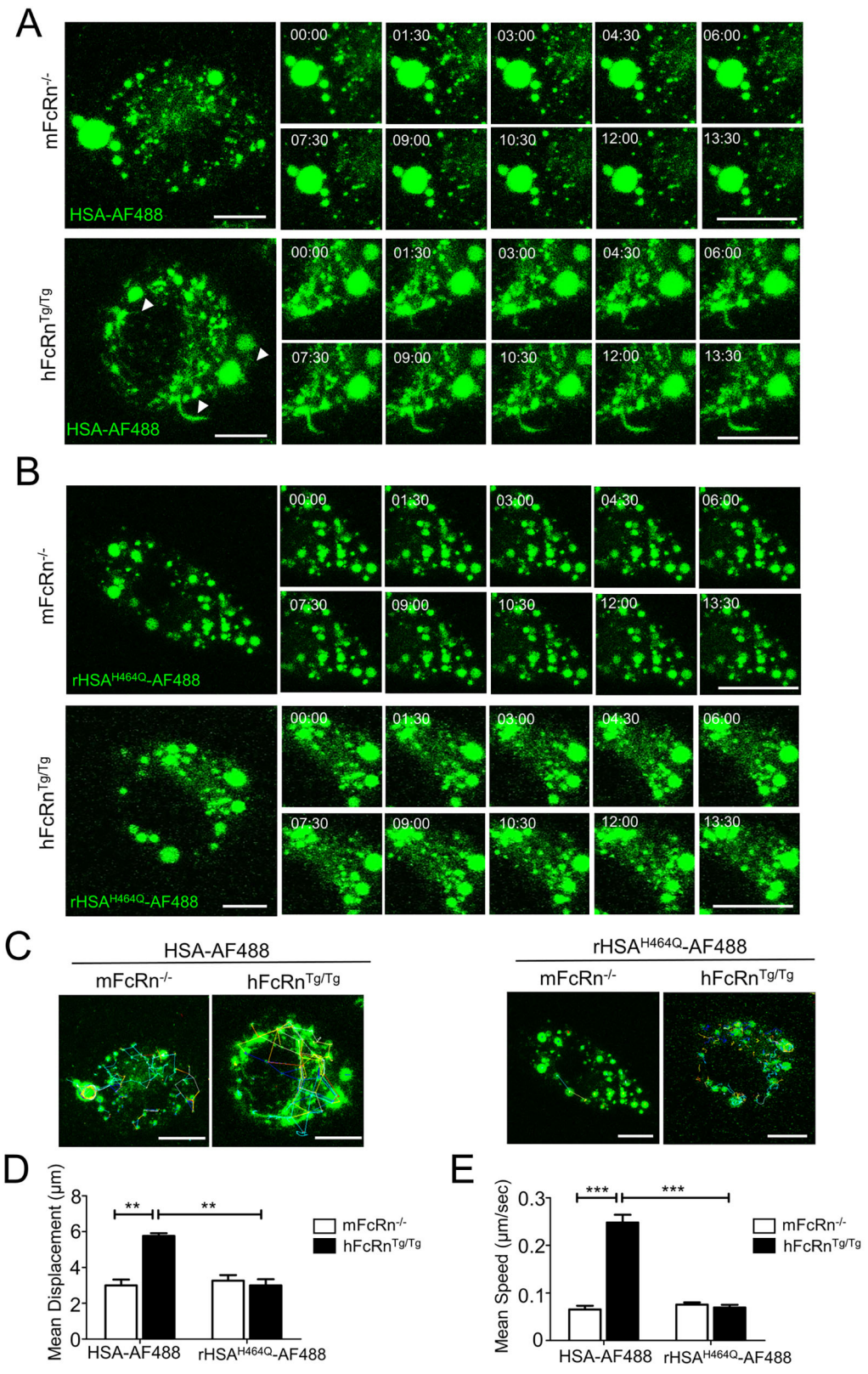

Fig. 6. HSA-loaded tubules emanating from macropinosomes in hFcRn$^{Tg/Tg}$ BMDMs but not in mFcRn$^{-/-}$ BMDMs. (A–E) mFcRn$^{-/-}$ and hFcRn$^{Tg/Tg}$ BMDMs were plated in eight-well chamber slides and rendered quiescent by culturing overnight in C-RPMI in the absence of mCSF-1. BMDMs were then incubated in 100 µg/ml HSA–AF488 or HSA^{H464Q}–AF488 in Leibovitz's medium supplemented with mCSF-1 for 10 min. BMDMs were washed in PBS and cells were imaged live in Leibovitz's medium using an SP8 confocal microscope over 20 min. (A,B) Snapshots of (A) HSA–AF488 or (B) HSA^{H464Q}–AF488 in mFcRn$^{-/-}$ and hFcRn$^{Tg/Tg}$ BMDMs. Images are presented as snapshots for every 1.5 min. (C,D) HSA–AF488 tracks were plotted using an ImageJ plugin, Trackmate. Tracks are shown in the images (C) and mean displacement and speed are presented in the bar graphs (D). Data represent the mean ±s.e.m. from three independent experiments. $^{**}P<0.01$, $^{***}P<0.001$ (unpaired two-tailed *t*-test). Scale bars: 10 µm.

(Carpinteria, CA). Whole-mouse serum was obtained from Justine Mintern (University of Melbourne, Bio21 Institute, Australia). CellMask Deep Red was purchased from Invitrogen (Thermo Fisher Scientific; C10046) and used at 1:1000 dilution in Leibovitz's medium.

Plasma-derived human serum albumin (HSA) and purified recombinant IgG_1 (BM4) were labelled with Alexa Fluor 488 (AF488) NHS ester (succinimidyl ester) (Life Technologies, A-20000) or Alexa Fluor 594 (AF594) NHS ester (succinimidyl ester) (Life Technologies, A-37572) respectively, according to the manufacturer's protocol. The recombinant FcRn non-binding albumin variant HSA^{H464Q} was generated and labelled with Alexa Fluor 488 (AF488) NHS ester (succinimidyl ester) (Life Technologies, A-20000) (rHSA^{H464Q}–AF488).

Journal of Cell Science (2020) 133, jcs235416. doi:10.1242/jcs.235416

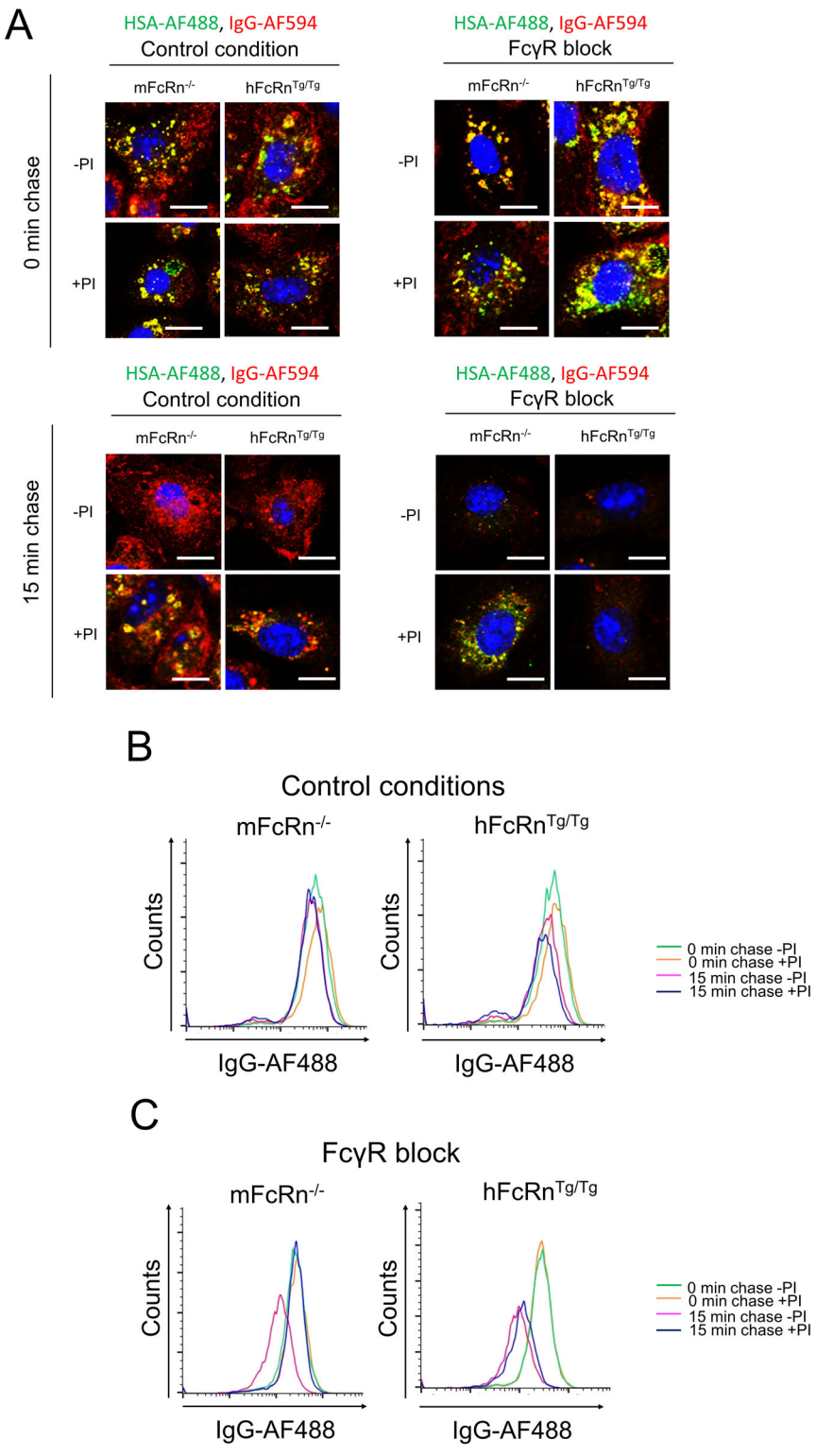

Fig. 7. Monomeric IgG can be recycled by FcRn in the absence of FcγR binding. (A–C) mFcRn$^{-/-}$ and hFcRn$^{Tg/Tg}$ BMDMs were plated in eight-well chamber slides and rendered quiescent by culturing overnight in C-RPMI in the absence of mCSF-1. The following day, cells were incubated in C-RPMI supplemented with either protease inhibitors (PI) or 0.01% DMSO (carrier control) for 4.5 h. To block FcγR, the relevant samples were incubated with mouse serum (1:100 dilution in C-RPMI) for 30 min on ice and washed with PBS. BMDMs were incubated with 100 µg/ml HSA–AF488 and IgG–AF594 or IgG–AF488 for the FACS, in the presence or absence of protease inhibitors, and mouse serum for the FcγR block experiments, in serum-free media (SFM) supplemented with mCSF-1 for 15 min. BMDMs were then washed in PBS, fixed in 4% PFA immediately (0 min chase) or chased in SFM containing either protease inhibitors (PI) or DMSO (carrier control) for 15 min, then fixed in 4% PFA, as indicated. (A) Confocal images of HSA–AF488 (green), IgG (red) and DAPI (blue) in mFcRn$^{-/-}$ and hFcRn$^{Tg/Tg}$ BMDMs at 0 min and 15 min time points. (B,C) mFcRn$^{-/-}$ and hFcRn$^{Tg/Tg}$ BMDMs containing IgG–AF488 under (B) control conditions and (C) FcγR block conditions at 0 and 15 min chase time points. Total fluorescence in cells was analysed by FACS. Histograms were overlaid in FlowJo. Scale bars: 10 µm.

Mice

FcRn$^{-/-}$ mice, which harbour a knockout allele of the mouse FcRn α-chain (*Fcgrt*^{tm1Dcr}), and FcRn$^{-/-}$ hFcRn (line 276) Tg mice (hFcRn$^{Tg/Tg}$), which have the null mutation for the mouse FcRn gene and a transgene expressing the human FcRn α-chain under the control of the β-actin promoter (Chaudhury et al., 2003), were purchased from Jackson Laboratory (Bar Harbour, ME) and mouse colonies established and maintained under specific pathogen-free conditions in the animal facility of Bio21 Institute, University of Melbourne. All experiments carried out on animals were approved by the Institutional Animal Care and Use Committee.

Isolation of primary mouse BMDMs

mFcRn$^{-/-}$ and hFcRn$^{Tg/Tg}$ mice (8 to 10 weeks of age) were killed by CO_2 asphyxiation, and BMDMs were generated as previously described (Lim et al., 2012). Cells were seeded in eight-well removable chamber slides (Ibidi, Germany) at 0.3×10^5 cells/well.

Journal of Cell Science (2020) 133, jcs235416. doi:10.1242/jcs.235416

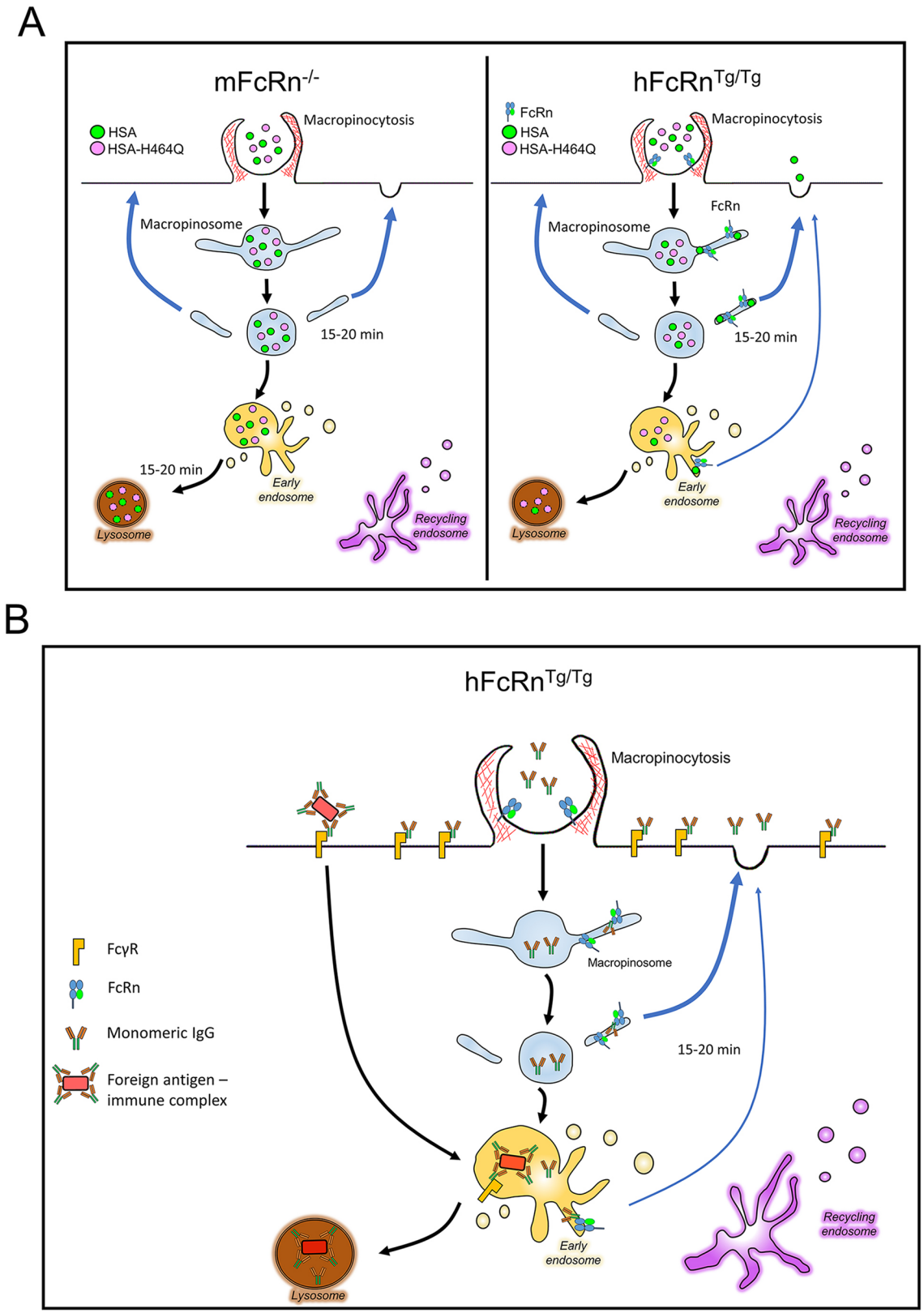

Fig. 8. Model of HSA and IgG recycling by hFcRn in BMDMs. (A) In BMDMs deficient in FcRn, HSA is rapidly degraded in late endosomes/lysosomes within 15–20 min after uptake by macropinocytosis. In the presence of hFcRn, internalised wild-type HSA (green), but not the HSA^{H464Q} mutant (purple) associates with FcRn in newly formed macropinosomes and enters the tubular elements of the macropinosome that pinch off for rapid recycling to the cell surface. Excess HSA not bound to FcRn remains in the body of the maturating macropinosome and is rapidly degraded, most likely owing to fusion with late endosomes/lysosomes. (B) Monomeric IgG is bound to FcγR on the cell surface of BMDMs with a long residence time. Unlike monomeric IgG, IgG that forms immune complexes binds FcγR and is rapidly internalised via clathrin-mediated endocytosis and transported to late endosomes/lysosomes for degradation. Excess monomeric IgG not bound to FcγR can be internalised by macropinocytosis and be rapidly recycled via FcRn to the cell surface.

HSA and IgG recycling assays

BMDMs were initially starved in C-RPMI [Roswell Park Memorial Institute media (RPMI) supplemented with 10% (v/v) fetal calf serum (FCS), 2 nM glutamine and 100 units/µl penicillin and 0.1% streptomycin (complete RPMI)] overnight in a humidified 10% CO_2 incubator at 37°C. On the next day, monolayers were incubated with either 0.01% DMSO (carrier control) or protease inhibitors in C-RPMI for 4.5 h at 37°C prior to the pulse-chase experiment. The protease inhibitor cocktail (Sigma Aldrich, P1860) contains apotinin, bestatin, E-64, luepeptin and pepstatin A. After 4.5 h, monolayers were washed with PBS buffer three times and pulsed with either HSA–AF488, rHSA^{H464Q}–AF488, IgG–AF594 or DQ–BSA (100 µg/ml) diluted in C-RPMI supplemented with mCSF-1 (50 ng/ml) in the presence of either 0.01% DMSO or protease inhibitors for 15 min at 37°C. Cell monolayers were then washed 6 times with PBS and chased for 0 min and 15 min in C-RPMI in the presence of either 0.01% DMSO carrier or protease inhibitors.

To quantify HSA recycling, BMDMs grown in six-well plates, were pulsed for 15 min with ligand as above, washed six times with PBS and fresh medium (500 µl) added to the cell monolayers. Conditioned medium was collected after the chase period and centrifuged at 21,130 ***g*** for 1 min to remove any cell debris. For cell lysates, monolayers were washed in PBS and lysed in 100 µl of RIPA buffer. 5% of the conditioned medium and 10% of cell lysate from each sample were analysed by immunoblotting. The levels of HSA in the conditioned medium were normalised to the input of cell lysates. The percentage of HSA recycled was calculated by dividing levels of normalised HSA in the conditioned medium by the total HSA levels in the cell lysates at the beginning of the chase period (0 min+protease inhibitors condition).

Confocal microscopy

Monolayers grown on coverslips were fixed in 4% paraformaldehyde (PFA) for 15 min at room temperature, followed by quenching in 50 mM NH_4Cl in PBS for 10 min at room temperature. Cells were permeablised with 0.1% Triton X-100 in PBS for 4 min and blocked in blocking solution (5% FCS and 0.02% sodium azide in PBS) for at least 30 min to reduce unspecific binding. Cells were incubated with primary antibodies diluted in blocking solution for 1–2 h at room temperature and washed six times in PBS. Diluted fluorochrome-conjugated secondary antibodies were added to monolayers and incubated for 30 min at room temperature and then washed six times in PBS. Coverslips were washed in milli-Q water before mounting in Mowoil [10% (w/v) Hopval 5-88, 25% (w/v) glycerol and 0.1 M Tris in milli-Q water]. Confocal microscopy was performed using a Leica SP8 system. Images were collected sequentially for multicolour imaging using a 63×/1.4 NA HCX PL APO CS oil immersion objective. GFP and Alexa Fluor 488 were excited with the 488-nm line of an argon laser, Alexa Fluor 568 and 594 were excited with a 543-nm HeNe laser, Alexa Fluor 647 was excited with a 633-nm HeNe laser, and DAPI with a 405-nm UV laser. Images were collected with pixel dimensions of at least 512×512. For multicolour labelling, images were collected independently.

Live-cell imaging

For live-cell imaging, cells were grown as monolayers in 35 mm µ-dishes (Ibidi, Germany). Cells were pulsed with either HSA–AF488 or HSA^{H464Q}–AF488 in the presence of mCSF-1 for 5 min, washed three times with PBS, and Leibovitz's L15 medium (#21083027, Life Technologies) was added for imaging purpose. Image acquisition were performed using a Leica SP8 confocal system using a 63×/1.4 NA objective at 12 s intervals. Live-cell imaging results were analysed and prepared using ImageJ and TrackMate plugin.

Immunoblotting

Cells were prepared in RIPA buffer [50 mM Tris-HCl, pH 7.3, 150 mM NaCl, 0.1 mM EDTA, 1% (w/v) sodium deoxycholate, 1% (v/v) Triton X-100, 0.2% (w/v) NaF and 100 µM Na_3VO_4] supplemented with Complete mini protease inhibitors (Sigma Aldrich). Cell lysates were incubated on ice for 10 min and centrifuged for 10 min at 16,000 ***g***. Protein concentrations were determined with a Bradford assay prior to SDS-PAGE. Proteins were resolved by SDS-PAGE (Life Technologies) and transferred onto Immobilon-P PVDF membrane (Millipore) at 30 V overnight at 4°C. The membrane was blocked by drying at 37°C. The membrane was incubated with primary antibodies diluted in 5% skim milk in PBS for 1 h and then washed three times for 10 min each in 0.1% (v/v) Tween 20 in PBS. HRP-conjugated secondary antibodies were then added to the membrane for 1 h and washed as above. Bound antibodies were detected through chemiluminescence and captured using the BioRad ChemiDOC imager (California, USA). Densitometry of the protein bands were measured using BioRad ImageLab program.

Flow cytometry

Cells were analysed at a medium flow rate in an LSRFortessa flow cytometer, equipped with 405 nm, 488 nm, 561 nm and 640 nm lasers (BD Biosciences). Approximately 10,000 events were collected, using a forward scatter threshold of 5000.

Quantification of colocalisation and statistical analysis

Quantification of the colocalisation between cargo and fluorescent organelle markers was performed using a custom macro developed in the open-source software Fiji (Schindelin et al., 2012) (version 1.49r), as previously described (Toh et al., 2018). Briefly, each file was imported with the Bio-Formats plugin to the workspace as an image stack containing multiple channels. Each channel was binarised using the Moments algorithm (Tsai, 1985), which selects a threshold value, such that the first three image moments are preserved between the original and the filtered image; these threshold values were independently recalculated for each image stack in the dataset. Using the thresholded channels as inputs, the organelle-based colocalisation plugin (OBCOL; Woodcroft et al., 2009) was used to calculate pixel overlap between detected objects in the cargo and organelle channels, where the object size was chosen to be at least 5 pixels. The per-image percentage colocalisation of cargo with organelle was then defined using the number of pixels that overlap with organelle marker according to:

$$\frac{\sum(overlap)}{\sum(cargo\ only)+\sum(overlap)}\times 100\%.$$

All analyses included samples from three or more independent experiments.

Data represent the mean±s.e.m. from three independent experiments, where for each experiment, an average value was determined from two to five images (each containing eight or more cells) for each time point and analysed by an unpaired two-tailed Student's *t*-test. $P<0.05$(*) was considered significant, $P<0.01$ (**), highly significant and $P<0.001$ (***), very highly significant. An absence of a P value indicates that the differences were not significant.

Acknowledgements

Confocal microscopy was performed at the Biological Optical Microscopy Platform (BOMP) at the University of Melbourne. We gratefully acknowledge Fiona Houghton (Department of Biochemistry and Molecular BIology, Bio21 Institute, University of Melbourne) for expert technical advice, and Shirley Taylor for the generation of fluorescent conjugates.

Competing interests

J.C., S.K.D., G.T.B. and A.M.V. are employees of CSL Limited and are able to partake in employee share option schemes. Research funding from CSL Limited is provided through an Australian Research Council linkage grant collaboration.

Author contributions

Conceptualization: S.K.D., A.M.V., P.A.G.; Methodology: W.H.T., J.L., J.C., P.A.G.; Validation: P.A.G.; Formal analysis: W.H.T., G.T.B.; Investigation: W.T., J.L., I.S.M., P.A.G.; Writing - original draft: W.H.T., P.A.G.; Writing - review & editing: W.H.T., J.L., I.S.M., J.C., S.K.D., A.M.V., P.A.G.; Supervision: A.M.V., P.A.G.; Funding acquisition: P.A.G.

Funding

This work was supported by funding for a Linkage grant from the Australian Research Council (LP106010137). I.S.M. was supported by a University of Melbourne International Postgraduate Award.

Supplementary information

Supplementary information available online at http://jcs.biologists.org/lookup/doi/10.1242/jcs.235416.supplemental

References

Akilesh, S., Christianson, G. J., Roopenian, D. C. and Shaw, A. S. (2007). Neonatal FcR expression in bone marrow-derived cells functions to protect serum IgG from catabolism. *J. Immunol.* **179**, 4580-4588. doi:10.4049/jimmunol.179.7.4580

Andersen, J. T., Dalhus, B., Cameron, J., Daba, M. B., Plumridge, A., Evans, L., Brennan, S. O., Gunnarsen, K. S., Bjørås, M., Sleep, D. et al. (2012). Structure-based mutagenesis reveals the albumin-binding site of the neonatal Fc receptor. *Nat. Commun.* **3**, 610. doi:10.1038/ncomms1607

Anderson, C. L. (2014). There's been a flaw in our thinking. *Front. Immunol.* **5**, 540. doi:10.3389/fimmu.2014.00540

Bryant, D. M., Kerr, M. C., Hammond, L. A., Joseph, S. R., Mostov, K. E., Teasdale, R. D. and Stow, J. L. (2007). EGF induces macropinocytosis and SNX1-modulated recycling of E-cadherin. *J. Cell Sci.* **120**, 1818-1828. doi:10.1242/jcs.000653

Buckley, C. M., Gopaldass, N., Bosmani, C., Johnston, S. A., Soldati, T., Insall, R. H. and King, J. S. (2016). WASH drives early recycling from macropinosomes and phagosomes to maintain surface phagocytic receptors. *Proc. Natl. Acad. Sci. USA* **113**, E5906-E5915. doi:10.1073/pnas.1524532113

Burmeister, W. P., Gastinel, L. N., Simister, N. E., Blum, M. L. and Bjorkman, P. J. (1994a). Crystal structure at 2.2 Å resolution of the MHC-related neonatal Fc receptor. *Nature* **372**, 336-343. doi:10.1038/372336a0

Burmeister, W. P., Huber, A. H. and Bjorkman, P. J. (1994b). Crystal structure of the complex of rat neonatal Fc receptor with Fc. *Nature* **372**, 379-383. doi:10.1038/372379a0

Chaudhury, C., Mehnaz, S., Robinson, J. M., Hayton, W. L., Pearl, D. K., Roopenian, D. C. and Anderson, C. L. (2003). The major histocompatibility complex-related Fc receptor for IgG (FcRn) binds albumin and prolongs its lifespan. *J. Exp. Med.* **197**, 315-322. doi:10.1084/jem.20021829

Chia, J., Louber, J., Glauser, I., Taylor, S., Bass, G. T., Dower, S. K., Gleeson, P. A. and Verhagen, A. M. (2018). Half-life extended recombinant coagulation factor IX-albumin fusion protein is recycled via the FcRn-mediated pathway. *J. Biol. Chem.* **293**, 6363-6373. doi:10.1074/jbc.M117.817064

Condon, N. D., Heddleston, J. M., Chew, T.-L., Luo, L., McPherson, P. S., Ioannou, M. S., Hodgson, L., Stow, J. L. and Wall, A. A. (2018). Macropinosome formation by tent pole ruffling in macrophages. *J. Cell Biol.* **217**, 3873-3885. doi:10.1083/jcb.201804137

Cullen, P. J. and Steinberg, F. (2018). To degrade or not to degrade: mechanisms and significance of endocytic recycling. *Nat. Rev. Mol. Cell Biol.* **19**, 679-696. doi:10.1038/s41580-018-0053-7

Daro, E., Pulendran, B., Brasel, K., Teepe, M., Pettit, D., Lynch, D. H., Vremec, D., Robb, L., Shortman, K., McKenna, H. J. et al. (2000). Polyethylene glycol-modified GM-CSF expands CD11b(high)CD11c(high) but notCD11b(low)CD11c(high) murine dendritic cells in vivo: a comparative analysis with Flt3 ligand. *J. Immunol.* **165**, 49-58. doi:10.4049/jimmunol.165.1.49

Diment, S. and Stahl, P. (1985). Macrophage endosomes contain proteases which degrade endocytosed protein ligands. *J. Biol. Chem.* **260**, 15311-15317.

Guilliams, M., Bruhns, P., Saeys, Y., Hammad, H. and Lambrecht, B. N. (2014). The function of Fcgamma receptors in dendritic cells and macrophages. *Nat. Rev. Immunol.* **14**, 94-108. doi:10.1038/nri3582

Kerr, M. C., Lindsay, M. R., Luetterforst, R., Hamilton, N., Simpson, F., Parton, R. G., Gleeson, P. A. and Teasdale, R. D. (2006). Visualisation of macropinosome maturation by the recruitment of sorting nexins. *J. Cell Sci.* **119**, 3967-3980. doi:10.1242/jcs.03167

Koivusalo, M., Welch, C., Hayashi, H., Scott, C. C., Kim, M., Alexander, T., Touret, N., Hahn, K. M. and Grinstein, S. (2010). Amiloride inhibits macropinocytosis by lowering submembranous pH and preventing Rac1 and Cdc42 signaling. *J. Cell Biol.* **188**, 547-563. doi:10.1083/jcb.200908086

Kuo, T. T., Baker, K., Yoshida, M., Qiao, S.-W., Aveson, V. G., Lencer, W. I. and Blumberg, R. S. (2010). Neonatal Fc receptor: from immunity to therapeutics. *J. Clin. Immunol.* **30**, 777-789. doi:10.1007/s10875-010-9468-4

Lim, J. P. and Gleeson, P. A. (2011). Macropinocytosis: an endocytic pathway for internalising large gulps. *Immunol. Cell Biol.* **89**, 836-843. doi:10.1038/icb.2011.20

Lim, J. P., Wang, J. T. H., Kerr, M. C., Teasdale, R. D. and Gleeson, P. A. (2008). A role for SNX5 in the regulation of macropinocytosis. *BMC Cell Biol.* **9**, 58. doi:10.1186/1471-2121-9-58

Lim, J. P., Teasdale, R. D. and Gleeson, P. A. (2012). SNX5 is essential for efficient macropinocytosis and antigen processing in primary macrophages. *Biol. Open* **1**, 904-914. doi:10.1242/bio.20122204

Lim, J. P., Gosavi, P., Mintern, J. D., Ross, E. M. and Gleeson, P. A. (2015). Sorting nexin 5 selectively regulates dorsal-ruffle-mediated macropinocytosis in primary macrophages. *J. Cell Sci.* **128**, 4407-4419. doi:10.1242/jcs.174359

Mahmoud, I. S., Louber, J., Dower, S. K., Verhagen, A. M. and Gleeson, P. A. (2017). Signal dependent transport of a membrane cargo from early endosomes to recycling endosomes. *Eur. J. Cell Biol.* **96**, 418-431. doi:10.1016/j.ejcb.2017.06.005

Martin, W. L., West, A. P., Jr., Gan, L. and Bjorkman, P. J. (2001). Crystal structure at 2.8 Å of an FcRn/heterodimeric Fc complex: mechanism of pH-dependent binding. *Mol. Cell* **7**, 867-877. doi:10.1016/S1097-2765(01)00230-1

Maxfield, F. R. and McGraw, T. E. (2004). Endocytic recycling. *Nat. Rev. Mol. Cell Biol.* **5**, 121-132. doi:10.1038/nrm1315

McNally, K. E., Faulkner, R., Steinberg, F., Gallon, M., Ghai, R., Pim, D., Langton, P., Pearson, N., Danson, C. M., Nägele, H. et al. (2017). Retriever is a multiprotein complex for retromer-independent endosomal cargo recycling. *Nat. Cell Biol.* **19**, 1214-1225. doi:10.1038/ncb3610

Molfetta, R., Quatrini, L., Gasparrini, F., Zitti, B., Santoni, A. and Paolini, R. (2014). Regulation of fc receptor endocytic trafficking by ubiquitination. *Front. Immunol.* **5**, 449. doi:10.3389/fimmu.2014.00449

Montoyo, H. P., Vaccaro, C., Hafner, M., Ober, R. J., Mueller, W. and Ward, E. S. (2009). Conditional deletion of the MHC class I-related receptor FcRn reveals the sites of IgG homeostasis in mice. *Proc. Natl. Acad. Sci. USA* **106**, 2788-2793. doi:10.1073/pnas.0810796106

Petkova, S. B., Akilesh, S., Sproule, T. J., Christianson, G. J., Al Khabbaz, H., Brown, A. C., Presta, L. G., Meng, Y. G. and Roopenian, D. C. (2006). Enhanced half-life of genetically engineered human IgG1 antibodies in a humanized FcRn mouse model: potential application in humorally mediated autoimmune disease. *Int. Immunol.* **18**, 1759-1769. doi:10.1093/intimm/dxl110

Racoosin, E. L. and Swanson, J. A. (1989). Macrophage colony-stimulating factor (rM-CSF) stimulates pinocytosis in bone marrow-derived macrophages. *J. Exp. Med.* **170**, 1635-1648. doi:10.1084/jem.170.5.1635

Roopenian, D. C. and Akilesh, S. (2007). FcRn: the neonatal Fc receptor comes of age. *Nat. Rev. Immunol.* **7**, 715-725. doi:10.1038/nri2155

Roopenian, D. C., Christianson, G. J., Sproule, T. J., Brown, A. C., Akilesh, S., Jung, N., Petkova, S., Avanessian, L., Choi, E. Y., Shaffer, D. J. et al. (2003). The MHC class I-like IgG receptor controls perinatal IgG transport, IgG homeostasis, and fate of IgG-Fc-coupled drugs. *J. Immunol.* **170**, 3528-3533. doi:10.4049/jimmunol.170.7.3528

Roopenian, D. C., Christianson, G. J. and Sproule, T. J. (2010). Human FcRn transgenic mice for pharmacokinetic evaluation of therapeutic antibodies. *Methods Mol. Biol.* **602**, 93-104. doi:10.1007/978-1-60761-058-8_6

Santambrogio, L., Sato, A. K., Carven, G. J., Belyanskaya, S. L., Strominger, J. L. and Stern, L. J. (1999). Extracellular antigen processing and presentation by immature dendritic cells. *Proc. Natl. Acad. Sci. USA* **96**, 15056-15061. doi:10.1073/pnas.96.26.15056

Schindelin, J., Arganda-Carreras, I., Frise, E., Kaynig, V., Longair, M., Pietzsch, T., Preibisch, S., Rueden, C., Saalfeld, S., Schmid, B. et al. (2012). Fiji: an open-source platform for biological-image analysis. *Nat. Methods* **9**, 676-682. doi:10.1038/nmeth.2019

Steinberg, F., Gallon, M., Winfield, M., Thomas, E. C., Bell, A. J., Heesom, K. J., Tavaré, J. M. and Cullen, P. J. (2013). A global analysis of SNX27-retromer assembly and cargo specificity reveals a function in glucose and metal ion transport. *Nat. Cell Biol.* **15**, 461-471. doi:10.1038/ncb2721

Swanson, J. A. (2008). Shaping cups into phagosomes and macropinosomes. *Nat. Rev. Mol. Cell Biol.* **9**, 639-649. doi:10.1038/nrm2447

Swanson, J. A. and Watts, C. (1995). Macropinocytosis. *Trends Cell Biol.* **5**, 424-428. doi:10.1016/S0962-8924(00)89101-1

Tesar, D. B. and Björkman, P. J. (2010). An intracellular traffic jam: Fc receptor-mediated transport of immunoglobulin G. *Curr. Opin. Struct. Biol.* **20**, 226-233. doi:10.1016/j.sbi.2010.01.010

Toh, W. H., Chia, P. Z. C., Hossain, M. I. and Gleeson, P. A. (2018). GGA1 regulates signal-dependent sorting of BACE1 to recycling endosomes, which moderates Aβ production. *Mol. Biol. Cell* **29**, 191-208. doi:10.1091/mbc.E17-05-0270

Tsai, W.-H. (1985). Moment-preserving thresolding: a new approach. *Comput. Vision, Graph. Image Process* **29**, 377-393. doi:10.1016/0734-189X(85)90133-1

van der Sluijs, P., Hull, M., Webster, P., Mâle, P., Goud, B. and Mellman, I. (1992). The small GTP-binding protein rab4 controls an early sorting event on the endocytic pathway. *Cell* **70**, 729-740. doi:10.1016/0092-8674(92)90307-X

van Kerkhof, P., Lee, J., McCormick, L., Tetrault, E., Lu, W., Schoenfish, M., Oorschot, V., Strous, G. J., Klumperman, J. and Bu, G. (2005). Sorting nexin 17 facilitates LRP recycling in the early endosome. *EMBO J.* **24**, 2851-2861. doi:10.1038/sj.emboj.7600756

Viuff, D., Antunes, F., Evans, L., Cameron, J., Dyrnesli, H., Thue Ravn, B., Stougaard, M., Thiam, K., Andersen, B., Kjærulff, S. et al. (2016). Generation of a double transgenic humanized neonatal Fc receptor (FcRn)/albumin mouse to study the pharmacokinetics of albumin-linked drugs. *J. Control. Release* **223**, 22-30. doi:10.1016/j.jconrel.2015.12.019

Ward, E. S. and Ober, R. J. (2009). Chapter 4: multitasking by exploitation of intracellular transport functions: the many faces of FcRn. *Adv. Immunol.* **103**, 77-115. doi:10.1016/S0065-2776(09)03004-1

Ward, E. S., Martinez, C., Vaccaro, C., Zhou, J., Tang, Q. and Ober, R. J. (2005). From sorting endosomes to exocytosis: association of Rab4 and Rab11 GTPases with the Fc receptor, FcRn, during recycling. *Mol. Biol. Cell* **16**, 2028-2038. doi:10.1091/mbc.e04-08-0735

West, M. A., Bretscher, M. S. and Watts, C. (1989). Distinct endocytotic pathways in epidermal growth factor-stimulated human carcinoma A431 cells. *J. Cell Biol.* **109**, 2731-2739. doi:10.1083/jcb.109.6.2731

Woodcroft, B. J., Hammond, L., Stow, J. L. and Hamilton, N. A. (2009). Automated organelle-based colocalization in whole-cell imaging. *Cytometry A* **75A**, 941-950. doi:10.1002/cyto.a.20786

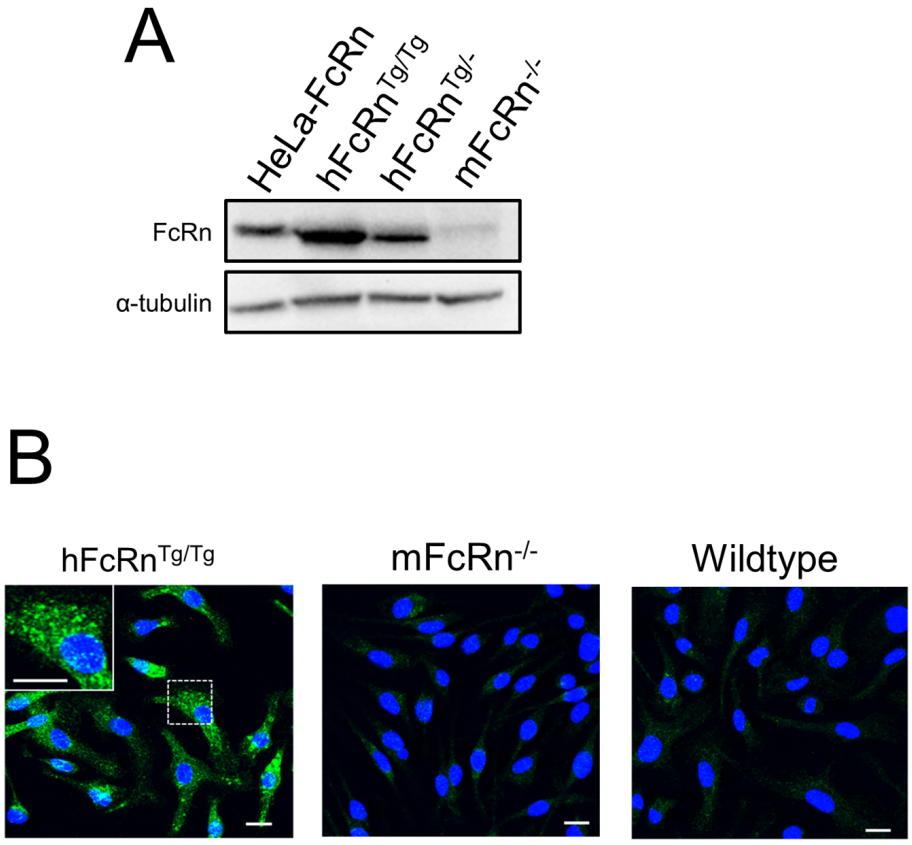

Figure S1 Analysis of BMDM from mFcRn$^{-/-}$ and hFcRn$^{Tg/Tg}$ mice

(A) *Immunoblotting*: BMDMs from either mFcRn-/-, hFcRn$^{Tg/Tg}$ or hFcRn$^{Tg/-}$ mice, as indicated, and HeLa cells stabling expressing hFcRn were lysed in reducing buffer and extracts resolved on 10 % PAGE gels. Proteins were then transferred onto PVDF membranes and probed with antibodies to human FcRn (rabbit polyclonal antibody (HPA012122), and mouse anti-α-tubulin antibodies, using a chemiluminescence detection system.

(B) *Detection of hFcRn in BMDMs by immunofluorescence:* BMDMs derived from mFcRn-/-, hFcRn$^{Tg/Tg}$ and wild type mice were fixed, stained for human FcRn with rabbit polyclonal antibody (HPA012122), followed by Alexa Fluor 488-conjugated anti-rabbit IgG. Nuclei were stained with DAPI (blue). Bars represent 5µm.

(C) *Alexa488-HSA internalisation in BMDMs:* FACS analysis to quantify the internalisation of Alexa488-HSA(HSA-AF488) in BMDMs derived from hFcRn$^{Tg/Tg}$ or mFcRn-/- mice. BMDM were incubated with HSA-AF488 for 15 min. Note the similar level of HSA-AF488 uptake by both hFcRn$^{Tg/Tg}$ and mFcRn-/- BMDMs.

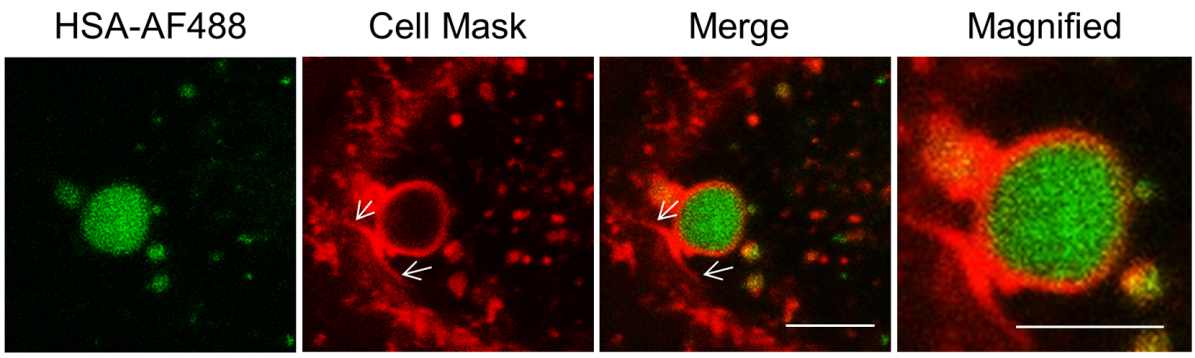

Figure S2: HSA-AF488 does not colocalise with tubules emanating from macropinosomes in BMDM from mFcRn$^{-/-}$ mice

mFcRn$^{-/-}$ BMDMs were plated in 8 well chamber slides and rendered quiescent by culturing overnight in C-RPMI in the absence of mCSF-1. BMDM were then incubated in Cell Mask Deep Red (1/1000 dilution), to stain the PM, and 100 µg/mL HSA-AF488 and in Leibovitz's media supplemented with mCSF-1 for 10 min. BMDM were washed in PBS and cells were imaged live in Leibovitz's media using an SP8 confocal microscope over 20 min. Images shown were snapshots of HSA-AF488 and Cell Mask Deep Red in mFcRn$^{-/-}$ BMDMs. Bar represents 10 µm.

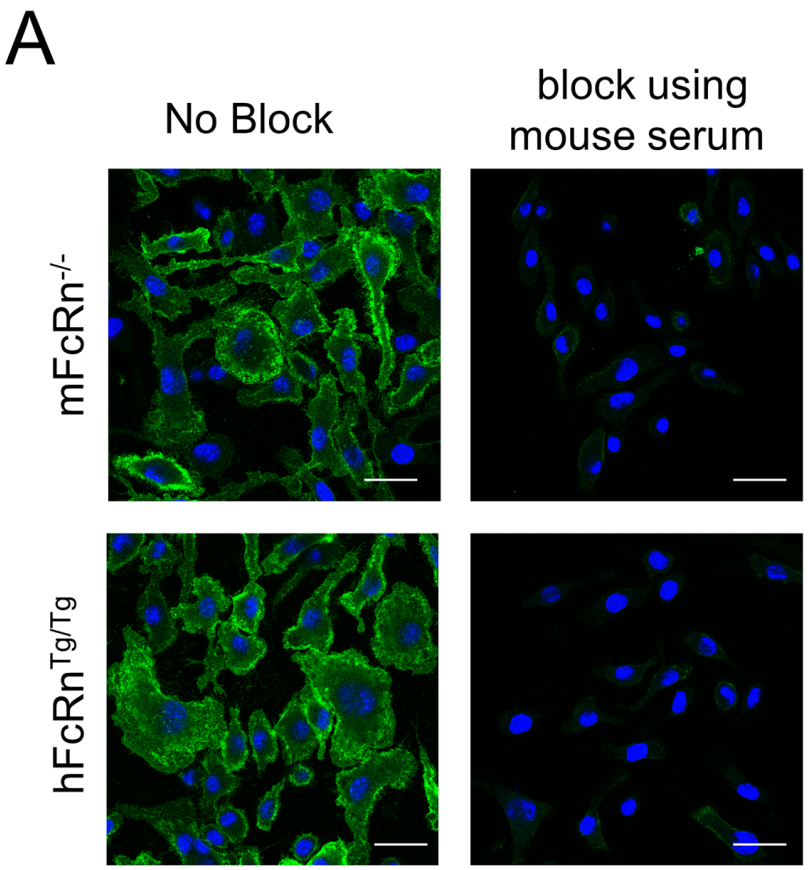

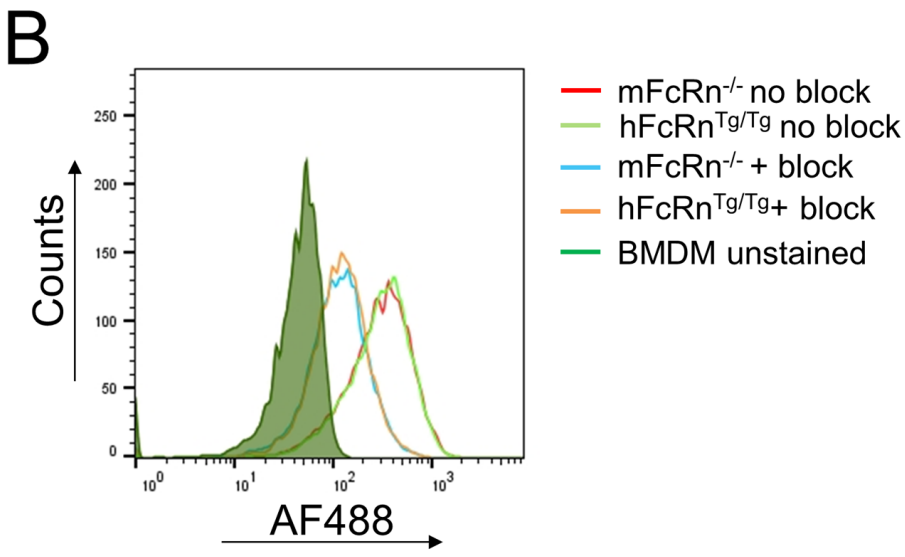

Figure S3: Mouse serum blocks IgG binding to FcγR on cell surface

(A-B) mFcRn$^{-/-}$ and hFcRn$^{Tg/Tg}$ BMDMs were plated in 8 well chamber slides and BMDMs were plated in 8 well chamber slides and rendered quiescent by culturing overnight in C-RPMI in the absence of mCSF-1. To block FcγR, BMDM were incubated with mouse serum (1/100 dilution in C-RPMI) for 30 min on ice and washed with PBS. BMDM were then incubated with 100 µg/mL IgG-AF488 in the presence or absence of mouse serum in serum-free media supplemented with mCSF-1 for 15 min. BMDM were then washed and fixed in 4% PFA.

(A) Confocal images of IgG-AF488 (green) and DAPI (blue) in mFcRn$^{-/-}$ and hFcRn$^{Tg/Tg}$ BMDMs in control conditions and FcγR block conditions. Bars represent 10 µm.

(B) mFcRn$^{-/-}$ and hFcRn$^{Tg/Tg}$ BMDMs containing IgG-AF488 under control condition and FcγR block condition. Total fluorescence was analysed by FACS and histograms were overlaid in Flowjo.

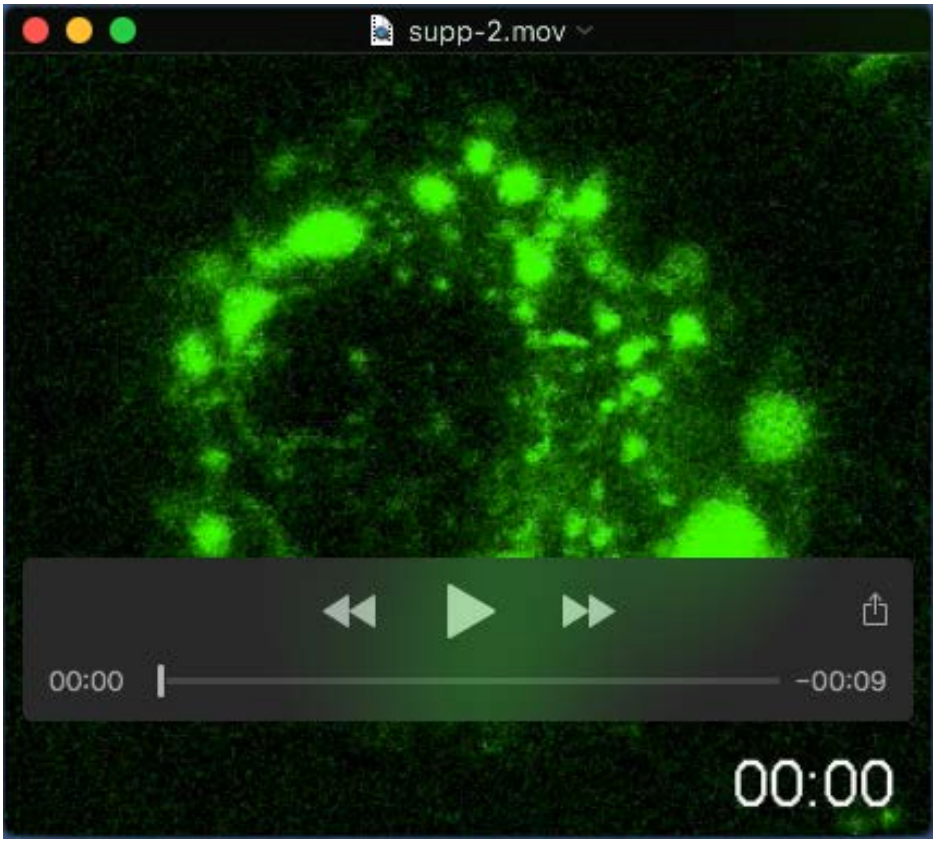

Movie 1: HSA-AF488 in hFcRn$^{Tg/Tg}$ BMDM

hFcRn$^{Tg/Tg}$ BMDMs were plated in 35mm Ibidi dishes and rendered quiescent by culturing overnight in C-RPMI in the absence of mCSF-1. BMDM were then incubated in 100 µg/mL HSA-AF488 in Leibovitz's media supplemented with 50 ng/mL mCSF-1 for 10 min. BMDM were washed in PBS and cells were imaged live in Leibovitz's media using an SP8 confocal microscope over 20 min. The delay between image capture was 12 sec.

Movie 2: HSA-AF488 in mFcRn$^{-/-}$ BMDM

mFcRn$^{-/-}$ BMDMs were plated in 35mm Ibidi dishes and rendered quiescent by culturing overnight in C-RPMI in the absence of mCSF-1. BMDM were then incubated in 100 µg/mL HSA-AF488 in Leibovitz's media supplemented with 50 ng/mL mCSF-1 for 10 min. BMDM were washed in PBS and cells were imaged live in Leibovitz's media using an SP8 confocal microscope over 20 min. The delay between image capture was 12 sec.

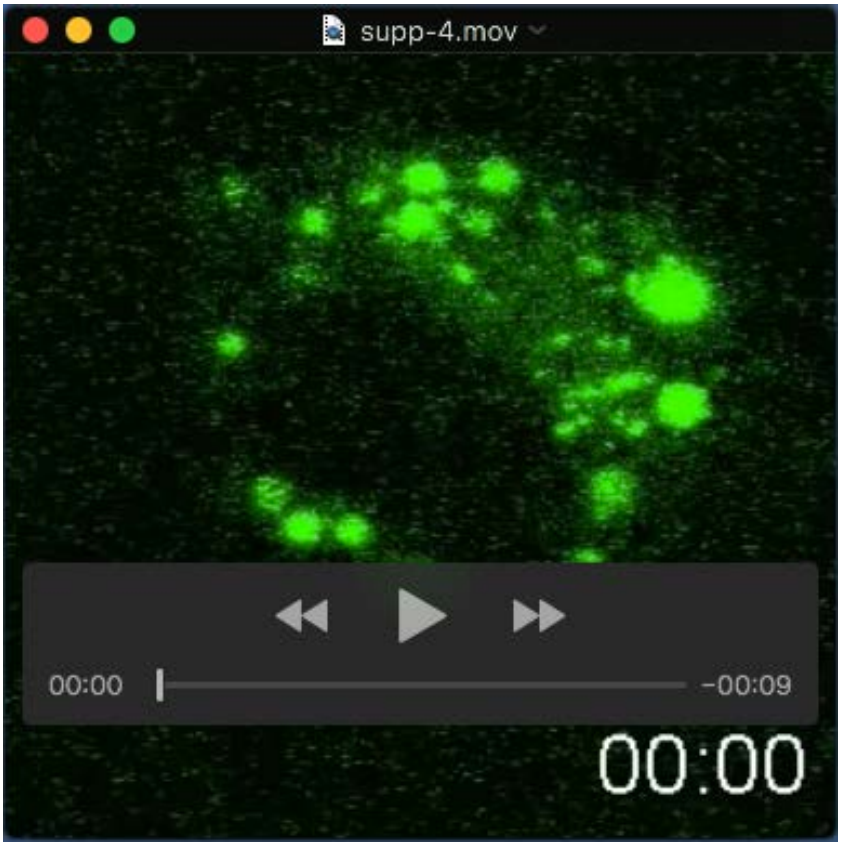

Movie 3: rHSA^{H464Q}-AF488 in hFcRn$^{Tg/Tg}$ BMDM

hFcRn$^{Tg/Tg}$ BMDMs were plated in 35mm Ibidi dishes and rendered quiescent by culturing overnight in C-RPMI in the absence of mCSF-1. BMDM were then incubated in 100 µg/mL rHSA^{H464Q}-AF488 in Leibovitz's media supplemented with 50 ng/mL mCSF-1 for 10 min. BMDM were washed in PBS and cells were imaged live in Leibovitz's media using an SP8 confocal microscope over 20 min. The delay between image capture was 12 sec.

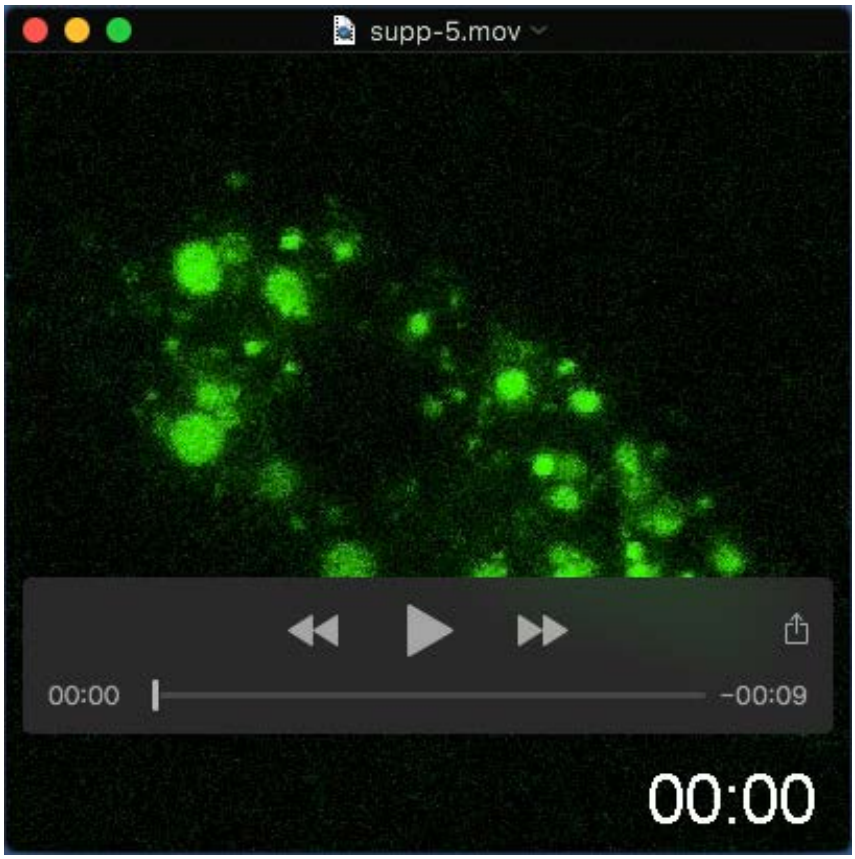

Movie 4: rHSA^{H464Q}-AF488 in mFcRn$^{-/-}$ BMDM

mFcRn$^{-/-}$ BMDMs were plated in 35mm Ibidi dishes and rendered quiescent by culturing overnight in C-RPMI in the absence of mCSF-1. BMDM were then incubated in 100 µg/mL HSA^{H464Q}-AF488 in Leibovitz's media supplemented with 50 ng/mL mCSF-1 for 10 min. BMDM were washed in PBS and cells were imaged live in Leibovitz's media using an SP8 confocal microscope over 20 min. The delay between image capture was 12 sec.

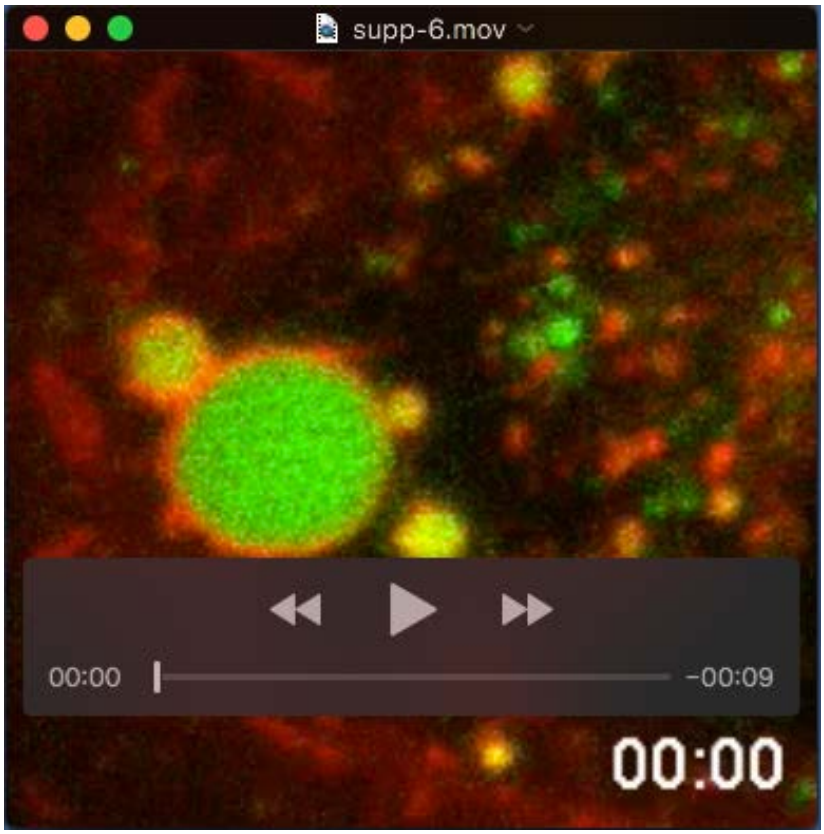

Movie 5: HSA-AF488 in mFcRn$^{-/-}$ BMDM labelled with CellMask Deep Red

mFcRn$^{-/-}$ BMDMs were plated in 35mm Ibidi dishes and rendered quiescent by culturing overnight in C-RPMI in the absence of mCSF-1. BMDM were then incubated in 100 µg/mL HSA-AF488 and cell mask deep red (1/1000 dilution) in Leibovitz's media supplemented with mCSF-1 for 10 min. BMDM were washed in PBS and cells were imaged live in Leibovitz's media using an SP8 confocal microscope over 20 min. The delay between image capture was 12 sec.